The Astrophysical Journal Supplement Series, 202:10 (22pp), 2012 September doi:10.1088/0067-0049/202/1/10

SPECTRAL OPTICAL MONITORING OF THE NARROW-LINE SEYFERT 1 GALAXY Ark 564

A. I. Shapovalova[1], L. Č. Popović[2,3], A. N. Burenkov[1], V. H. Chavushyan[4], D. Ilić[3,5], A. Kovačević[3,5], W. Kollatschny[6], J. Kovačević[2,3], N. G. Bochkarev[7], J. R. Valdes[4], J. Torrealba[4], J. León-Tavares[8], A. Mercado[9], E. Benítez[10], L. Carrasco[4], D. Dultzin[10], and E. de la Fuente[11]

[1] Special Astrophysical Observatory of the Russian AS, Nizhnij Arkhyz, Karachaevo-Cherkesia 369167, Russia; ashap@sao.ru
[2] Astronomical Observatory, Volgina 7, 11160 Belgrade 74, Serbia
[3] Isaac Newton Institute of Chile, Yugoslavia Branch, Belgrade, Serbia
[4] Instituto Nacional de Astrofísica, Óptica y Electrónica, Apartado Postal 51-216, 72000 Puebla, Mexico
[5] Department of Astronomy, Faculty of Mathematics, University of Belgrade, Studentski Trg 16, 11000 Belgrade, Serbia
[6] Institut für Astrophysik, Georg-August-Universität, Göttingen, Germany
[7] Sternberg Astronomical Institute, Moscow, Russia
[8] Aalto University Metsähovi Radio Observatory, Metsähovintie 114, FIN-02540 Kylmälä, Finland
[9] Universidad Politécnica de Baja California, Av. de la Industria 291, 21010 Mexicali, B.C., Mexico
[10] Instituto de Astronomía, Universidad Nacional Autónoma de México, Apartado Postal 70-264, México, D.F. 04510, Mexico
[11] Instituto de Astronomía y Meteorología, Dpto. de Física CUCEI, Universidad de Guadalajara, Av. Vallarta 2602, 44130 Guadalajara, Jalisco, Mexico
Received 2012 March 27; accepted 2012 July 2; published 2012 August 30

ABSTRACT

We present the results of a long-term (1999–2010) spectral optical monitoring campaign of the active galactic nucleus (AGN) Ark 564, which shows a strong Fe II line emission in the optical. This AGN is a narrow-line Seyfert 1 (NLS1) galaxy, a group of AGNs with specific spectral characteristics. We analyze the light curves of the permitted Hα, Hβ, optical Fe II line fluxes, and the continuum flux in order to search for a time lag between them. Additionally, in order to estimate the contribution of iron lines from different multiplets, we fit the Hβ and Fe II lines with a sum of Gaussian components. We find that during the monitoring period the spectral variation ($F_{\rm max}/F_{\rm min}$) of Ark 564 is between 1.5 for Hα and 1.8 for the Fe II lines. The correlation between the Fe II and Hβ flux variations is of higher significance than that of Hα and Hβ (whose correlation is almost absent). The permitted-line profiles are Lorentzian-like and do not change shape during the monitoring period. We investigate, in detail, the optical Fe II emission and find different degrees of correlation between the Fe II emission arising from different spectral multiplets and the continuum flux. The relatively weak and different degrees of correlations between permitted lines and continuum fluxes indicate a rather complex source of ionization of the broad-line emission region.

Key words: galaxies: active – galaxies: individual (Ark 564) – galaxies: Seyfert – line: profiles – quasars: emission lines

Online-only material: color figures

1. INTRODUCTION

Narrow-line Seyfert 1 (NLS1) galaxies were first introduced as a class of active galactic nuclei (AGNs) by Osterbrock & Pogge (1985). Their optical spectra show relatively narrow (FWHM $\leqslant$ 2000 km s^{-1}) permitted lines, which are narrower than in a typical Seyfert 1 galaxy. In particular, Osterbrock & Pogge (1985) showed that the permitted lines are only slightly broader than the forbidden ones and that a strong Fe II emission is present in the optical region of the spectrum. In addition, the [O III] λ5007/Hβ ratio, emitted in the narrow-line region (NLR), has a value that varies from 1 to 5 (Rodríguez-Ardila et al. 2000) instead of the universally adopted observed value for Seyfert 1s of around 10 (Rodríguez-Ardila et al. 2000), which is indicative of the presence of high-density gas. Osterbrock & Pogge (1985) pointed out that the Hβ equivalent widths in NLS1s are smaller than the typical values for normal Seyfert 1s, suggesting that these galaxies are not just normal Seyfert 1s seen at a particular viewing angle. Renewed interest in NLS1s arises from the discovery of their distinctive X-ray properties: they show a steep X-ray excess with a photon index of 3 below 100 keV, a steep hard X-ray continuum, and a rapid large-amplitude X-ray variability on timescales of minutes to hours (see Leighly 1999a, 1999b, 2000; Panessa et al. 2011, and references therein). Moreover, optical studies have established that NLS1s lie at one end of the Boroson & Green (1992) eigenvector 1 (EV1) and that they show a relatively strong Fe II emission and a weak [O III] emission (Boller et al. 1996). They also represent the "extreme Population A" objects (FWHM Hβ < 4000 km s^{-1}) as defined by the four-dimensional eigenvector 1 (4DE1) in Sulentic et al. (2007) and Marziani et al. (2010). 4DE1 involves four parameters, and NLS1 is "extreme" in all of them: they have the narrowest broad Hβ, strongest Fe II emission, strongest X-ray excess, and largest C IV blueshifts.

Arakelian 564 (Ark 564, IRAS 22403+2927, MGC +05-53-012) is a bright $V = 14.6$ mag (de Vaucouleurs et al. 1991), nearby NLS1 galaxy ($z = 0.02467$) with an X-ray luminosity of $L_{2-10\,{\rm keV}} = 2.4 \times 10^{43}$ erg s^{-1} (Turner et al. 2001). This AGN is one of the brightest NLS1s in the X-ray band (Boller et al. 1996; Collier et al. 2001; Smith et al. 2008), and it shows a soft excess below ~1.5 keV and a peculiar emission-line-like feature at 0.712 keV in the source rest frame (Matsumoto et al. 2004). The variations of the X-ray amplitude in the short-timescale light curve are very similar to those in the long-timescale light curve (Pounds et al. 2001), that is, in contrast to the stronger amplitude variability on longer timescales, which is a characteristic of broad-line Seyfert 1 (BLS1) galaxies. In the UV part of the spectrum, this galaxy shows intrinsic UV absorption lines (Crenshaw et al. 1999). In order to explore the variability characteristics of an NLS1 in different wavelength bands, a multiwavelength monitoring campaign of Ark 564 was conducted (Shemmer et al. 2001). The optical campaign covered the periods 1998 November–1999 November and 2000 May–2001 January, where the object was observed both photometrically (*UBVRI* filters) and spectrophotometrically (spectral coverage 4800–7300 Å; Shemmer et al. 2001). The data set and analysis are described in detail and compared with the simultaneous X-ray and UV campaigns (Shemmer et al. 2001). The results of this intensive variability multiwavelength campaign show that the optical continuum is not significantly correlated with the X-ray emission (Shemmer et al. 2001). The UV campaign, carried out with the *Hubble Space Telescope* (*HST*) on 2000 May 9 and 2000 July 8, is described in Collier et al. (2001). These authors found a small fractional variability amplitude of the continuum between 1365 Å and 3000 Å (around 6%), but reported that large-amplitude short-timescale flaring behavior is present, with trough-to-peak flux changes of about 18% in approximately 3 days (Collier et al. 2001). The wavelength-dependent continuum time delays in Ark 564 were detected, and these delays may indicate a stratified continuum reprocessing region (Collier et al. 2001).

Here, we present the long-term monitoring of Ark 564 in the optical part of the spectrum. We analyzed the variability in the permitted emission lines and the continuum in order to determine the size and structure of emitting regions of the permitted Balmer and Fe II lines. We placed particular emphasis on the strong Fe II lines of the Hβ spectral region, whose behavior is investigated in detail and discussed in this paper.

The paper is organized as follows. In Section 2, we describe the observations and data reduction procedures. In Section 3, we give an analysis of the spectral data. In Section 4, we explore the correlations between different lines and the continuum, as well as between different lines. In Section 5, we investigate in greater detail the Fe II variation. In Section 6, we discuss our results, and in Section 7, we provide our conclusions.

2. OBSERVATIONS AND DATA REDUCTION

Spectral monitoring of Ark 564 was carried out with the 6 m and 1 m telescopes of the SAO RAS (Russia, 1999–2010), the INAOE's 2.1 m telescope of the Guillermo Haro Observatory (GHO) at Cananea, Sonora, México (1999–2007), and the 2.1 m telescope of the Observatorio Astronómico Nacional at San Pedro Martir (OAN-SPM), Baja California, México (2005–2007). Spectra were taken with long-slit spectrographs equipped with CCDs. The typical observed wavelength range was 4000–7500 Å, the spectral resolution was $R = 5$–15 Å, and the signal-to-noise ratio (S/N) was >50 in the continuum near Hα and Hβ. In total, 100 blue and 55 red spectra were obtained during 120 nights. In the analysis, about 10% of the spectra were discarded for several different reasons, e.g., (1) large noise (S/N < 15 Å)—2001 August 29 (blue, red), 2001 October 8 (blue), 2001 October 9 (blue, red), taken with Zeiss (1 m) + CCD (1k × 1k); (2) large noise and badly corrected spectral sensitivity in the blue part—2006 June 28 (blue, red), 2006 August 29 (blue), 2006 August 30 (blue), 2009 August 14 (blue), 2009 October 11 (blue), taken with Zeiss (1m) + CCD (2k × 2k), noting here that the CCD (2k × 2k) sensitivity in the blue part is not good enough, since it is a red CCD; and (3) poor spectral resolution (R >20 Å)—2003 November 18, 2004 October 18, taken with the 2.1m GHO. Thus, our final data set consisted of 91 blue and 50 red spectra, which were used in further analysis.

From 1999 to 2003, spectral observations with the 1 m Zeiss telescope of the SAO were carried out with two different CCDs (the formats used were 1k × 1k or 530 × 580), and the Hα and Hβ spectral regions were observed separately. From 2004 to 2010 a CCD (2k × 2k, EEV CCD42-40) was used, allowing us to observe the entire wavelength range (4000–8000) Å with a spectral resolution of 8–10 Å. However, this CCD presents large sensitivity variations in the blue part of some spectra (i.e., bad S/N), which are badly corrected; thus, the blue region of these spectra was not used in our analysis.

From 2004 to 2007, the spectral observations with two Mexican 2.1 m telescopes were carried out with two observational setups. In the case of GHO observations, we used the following configurations: (1) with a grating of 150 l/mm (spectral resolution of $R = 15$ Å, a resolution similar to the observations of 1999–2003) and (2) with a grating of 300 l/mm (moderate spectral resolution of $R = 7.5$ Å). The similar spectral characteristics at the OAN-SPM were, respectively, obtained with the following configurations: (1) with a grating of 300 l/mm (spectral resolution of $R = 15$ Å) and (2) with a grating of 600 l/mm (moderate spectral resolution of $R = 7.5$ Å).

As a rule, observations were carried out with moderate resolution in the blue or red bands during the first night of each run. In order to cover Hα and Hβ at the same time, we used the lower resolution mode and observed the entire spectral range 4000–7500 Å; moderate resolution was adopted again for the following night. Since the shape of the continuum of active galaxies remains practically unchanged during adjacent nights, it was easy to match the blue and red bands obtained with the moderate resolution on different nights. To this end, we used the data obtained for the continuum from the low-dispersion spectra for the entire wavelength range. With this procedure, the photometric accuracy is thus considerably improved with respect to a match obtained by overlapping the extremes of the blue and the red continua (3%–5% instead of 5%–10%). Spectrophotometric standard stars were observed every night.

Information on the source of spectroscopic observations is listed in Table 1. The log of the spectroscopic observations is given in Table 2. Taking into account all observations, the mean sampling rate is 33.20 and the median rate is 2.95 days. The big difference between the mean and the median sampling rates is due to the big gaps in the variability campaign.

Spectrophotometric data reduction was carried out either with the software developed at the SAO RAS or with the IRAF package for the spectra obtained in México. The image reduction process included bias and flat-field corrections, cosmic-ray removal, two-dimensional wavelength linearization, sky spectrum subtraction, addition of the spectra for every night, and relative flux calibration based on observations of standard stars.

2.1. Absolute Calibration (Scaling) of the Spectra

The standard technique of flux calibrating the spectra (i.e., performing a comparison with stars of known spectral energy distribution) is not precise enough for the study of AGN variability, since even under good photometric conditions the accuracy of spectrophotometry is usually not better than 10%. Therefore, we used standard stars only to provide a relative flux calibration. Instead, for the absolute calibration, the observed fluxes of the forbidden, narrow emission lines are adopted for the scaling procedure of the AGN spectra since these fluxes are expected to be constant (Peterson 1993). From *HST* observations (Crenshaw et al. 2002) it was shown that the NLR in Ark 564 is about 0$''$.2 (95 pc), and this fact implies a constant [O III]λ5007 flux intensity during several hundred years. Consequently, the flux of this forbidden line should not

Table 1
Sources of Spectroscopic Observations

Observatory	Code	Tel. Aperture + Equipment	Aperture	Focus	No.	Period
1	2	3	4	5	6	7
SAO (Russia)	L(U)	6 m + UAGS	2.0 × 6.0	Prime	9	1999–2001
SAO (Russia)	L(N)	6 m + UAGS	2.0 × 6.0	Nasmith	1	1999 Oct 9
SAO (Russia)	Z1K	1 m + UAGS+CCD1K	4.0 × 19.8	Cassegrain	19	1999–2001
SAO (Russia)	Z2K	1 m + UAGS+CCD2K	4.0 × 4.0	Cassegrain	5	2006–2009
Gullermo Haro (México)	GHO	2.1 m + B&C	2.5 × 6.0	Cassegrain	74	2000–2007
San Pedro Martir (México)	SPM	2.1 m + B&C	2.5 × 6.0	Cassegrain	12	2005–2007

Notes. Column 1: observatory; Column 2: code assigned to each combination of telescope + equipment used throughout this paper; Column 3: telescope aperture and spectrograph; Column 4: projected spectrograph entrance apertures (slit width × slit length in arcsec); Column 5: focus of the telescope; Column 6: number of spectra obtained; Column 7: observation period.

have changed during our monitoring period. The scaling of the blue spectra was performed using the method of Van Groningen & Wanders (1992) modified by Shapovalova et al. (2004).[12] We will not repeat the scaling procedure here; we only note that the flux in the lines was determined after the subtraction of a linear continuum determined by the beginning and the end of a given spectral interval. This method allowed us to obtain a homogeneous set of spectra with the same wavelength calibration and the same [O III]λ5007 flux. The [O III]λ5007 flux in absolute units was taken from Shemmer et al. (2001): $F([\text{O III}]\lambda5007) = (2.4 \pm 0.1) \times 10^{-13}$ erg s^{-1} cm^{-2}. The spectra, obtained with 2.1 m telescopes in Mexico with a resolution of 12–15 Å, containing both Hα and Hβ regions, were scaled using the [O III]λ5007 line. However, some spectra of Ark 564 were obtained separately in the blue (Hβ) and red (Hα) wavelength bands, with a resolution of 8–10 Å. Usually, the red edge of the blue spectra and the blue edge of the red spectra overlap in an interval of 300 Å. Therefore, first the red spectra (17) were scaled using the continuum region overlapping with the blue ones. The latter were scaled with the [O III]λ5007 line. In these cases, the scaling uncertainty was about 5%–10%. Then, the scaling of the red spectra was refined using the mean flux in [O I]λ6300 (mean F[O I]λ6300 $\sim(1.93 \pm 0.24) \times 10^{-14}$), determined from low-dispersion spectra (R ∼12–15 Å). For three red spectra (JD:2452886.9, 2455058.5, and 245116.4) we have no blue spectrum in adjacent nights, and they were scaled using only the mean flux of the [O III]λ6300 line.

2.2. Unification of the Spectral Data

In order to investigate the long-term spectral variability of an AGN, it is necessary to conform a consistent, uniformed data set. Since observations were carried out with four different instruments, we must correct the line and continuum fluxes for aperture effects (Peterson & Collins 1983). To this effect, we determined a point-source correction factor φ given by the following expression (see Peterson et al. 1995, for a detailed discussion):

$$F(\text{H}\beta)_{\text{true}} = \varphi \cdot F(\text{H}\beta)_{\text{obs}},$$

where $F(\text{H}\beta)_{\text{obs}}$ is the observed Hβ flux and $F(\text{H}\beta)_{\text{true}}$ is the aperture-corrected Hβ flux. The contribution of the host galaxy to the continuum flux depends also on the aperture size. The continuum fluxes F(5235 Å) (in the observed frame) were corrected for different amounts of host-galaxy contamination according to the following expression (see Peterson et al. 1995):

$$F(5235\ \text{Å})_{\text{true}} = \varphi \cdot F(5235\ \text{Å})_{\text{obs}} - G(g),$$

where $F(5235\ \text{Å})_{\text{obs}}$ is the continuum flux at 5235 Å in the observed frame and $G(g)$ is an aperture-dependent correction factor used to account for the host-galaxy contribution. The GHO observing scheme (Table 1), which corresponds to a projected aperture (2$''$.5 × 6$''$) of the 2.1 m telescope, was adopted as standard (i.e., $\varphi = 1.0$, $G(g) = 0$ by definition). The correction factors φ and $G(g)$ are determined empirically by simulated aperture photometry of suitable images of the narrow-line emission and the starlight of the host galaxy in the same way as that given in Peterson et al. (1995). This procedure is accomplished empirically by comparing pairs of simultaneous observations from each of the given telescope data sets to that of the standard data set (as used in AGN Watch, e.g., Peterson et al. 1994, 1999, 2002). As noted in these papers, even after scaling the spectra to a common value of the [O III] 5007 flux, there are systematic differences between the light curves produced from the data obtained with different telescopes. Therefore, we propose correcting for small offsets between the light curves from different sources in a simple but effective fashion (e.g., Peterson et al. 2002, and references therein), attributing these small relative offsets to aperture effects (Peterson et al. 1995). The procedure also corrects for other unidentified systematic differences between data sets (for example, miscentering of the AGN nucleus in spectrograph aperture, etc.). In our paper, we take the GHO data as standard, because this data set contains the largest number of observed spectra. The correction factors φ and $G(g)$ are determined empirically by comparing pairs of nearly simultaneous observations from each of the given telescope data sets (L(U), SPM, Z1K, Z2K) to that of the GHO data set. In practice, intervals that we define as "nearly simultaneous" are typically of 1–2 days. Therefore, the variability on short timescales (<2 days) is suppressed. The point-source correction factors φ and $G(g)$ values for different samples are listed in Table 3. Using these factors, we recalibrated the observed fluxes of Hα, Hβ, Fe II 48,49, and continuum to a common scale corresponding to our standard aperture 2$''$.5 × 6$''$ (Table 4).

2.3. Measurements of the Spectra and Errors

From the scaled spectra, we determined the average flux in the blue continuum at the rest-frame wavelength ∼5100 Å by means of flux averages in the spectral interval 5094–5123 Å in the rest frame (Table 5). We also calculated the average flux in the red continuum at the rest-frame wavelength ∼6200 Å by

[12] See Appendix A of Shapovalova et al. (2004).

Table 2
The Log of Spectroscopic Observations

No.	UT Date	JD+ 2400000+	CODE	Aperture (arcsec)	Spectral Range (Å)	Resolution (Å)	Seeing (arcsec)
1	2	3	4	5	6	7	8
1	1999 Sep 2	51424.4	Z1K	4.0 × 19.8	4025–5825	7	2.0
2	1999 Sep 3	51425.4	L(U)	2.0 × 6.0	3620–6044	9	1.5
3	1999 Sep 4	51426.4	Z1K	4.0 × 19.8	4025–5825	7	2.0
4	1999 Sep 5	51427.3	L(U)	2.0 × 6.0	3650–6074	8	1.6
5	1999 Sep 5	51427.4	L(U)	2.0 × 6.0	4900–7324	9	1.6
6	1999 Oct 3	51455.2	L(U)	2.0 × 6.0	4320–5568	5	1.3
7	1999 Oct 3	51455.3	L(U)	2.0 × 6.0	6030–7278	5	1.3
8	1999 Oct 4	51456.2	L(U)	2.0 × 6.0	4320–5556	6	1.3
9	1999 Oct 4	51456.3	L(U)	2.0 × 6.0	6040–7276	5	1.3
10	1999 Oct 9	51461.3	L(N)	2.0 × 6.0	4240–6590	8	2.5
11	1999 Oct 13	51465.2	Z1K	4.0 × 19.8	4050–5850	6	2.0
12	1999 Nov 2	51485.3	Z1K	4.0 × 19.8	4025–5825	7	2.0
13	1999 Nov 3	51486.2	Z1K	4.0 × 19.8	4025–5825	7	2.0
14	1999 Nov 4	51487.2	Z1K	4.0 × 19.8	4025–5825	6	2.0
15	1999 Nov 5	51488.2	Z1K	4.0 × 19.8	4025–5825	8	2.0
16	1999 Nov 6	51489.2	Z1K	4.0 × 19.8	4025–5825	7	2.0
17	1999 Nov 30	51513.2	Z1K	4.0 × 19.8	4025–5825	7	2.0
18	1999 Dec 2	51515.2	Z1K	4.0 × 19.8	4050–5850	8	2.0
19	2000 May 28	51693.5	L(U)	2.0 × 6.0	3550–5974	8	1.6
20	2000 Jun 6	51702.4	Z1K	4.0 × 19.8	4020–5820	8	3.0
21	2000 Jul 8	51734.4	Z1K	4.0 × 19.8	4050–5850	8	3.0
22	2000 Jul 9	51735.4	Z1K	4.0 × 19.8	4050–5850	7	3.0
23	2000 Jul 10	51736.4	Z1K	4.0 × 19.8	4030–5830	7	3.0
24	2000 Oct 16	51833.7	GHO	2.5 × 6.0	4000–7300	12	2.3
25	2001 Aug 29	52151.5	Z1K	4.0 × 19.8	4040–5840	7	2.0
26	2001 Aug 29	52151.5	Z1K	4.0 × 19.8	5600–7290	8	2.0
27	2001 Oct 8	52191.2	Z1K	4.0 × 19.8	4050–5850	8	2.0
28	2001 Oct 9	52192.3	Z1K	4.0 × 19.8	4040–5840	7	2.0
29	2001 Oct 9	52192.4	Z1K	4.0 × 19.8	5640–7290	11	2.0
30	2001 Nov 23	52237.1	L(U)	2.0 × 6.0	3600–6024	10	3.5
31	2001 Nov 23	52236.6	GHO	2.5 × 6.0	4200–5960	8	2.5
32	2001 Nov 24	52237.6	GHO	2.5 × 6.0	6000–7360	9	1.5
33	2002 Aug 15	52501.8	GHO	2.5 × 6.0	4270–5840	10	2.5
34	2002 Aug 17	52503.9	GHO	2.5 × 6.0	5700–7460	10	2.0
35	2002 Nov 11	52589.7	GHO	2.5 × 6.0	4300–6060	8	4.5
36	2002 Nov 12	52590.7	GHO	2.5 × 6.0	5700–7460	10	2.7
37	2002 Nov 13	52591.7	GHO	2.5 × 6.0	5700–7460	9	2.7
38	2002 Nov 14	52592.7	GHO	2.5 × 6.0	3800–7100	10	2.7
39	2002 Dec 10	52618.6	GHO	2.5 × 6.0	4300–6060	8	1.5
40	2002 Dec 11	52619.6	GHO	2.5 × 6.0	5700–7460	9	1.8
41	2002 Dec 12	52620.6	GHO	2.5 × 6.0	3800–7100	13	1.8
42	2003 Sep 4	52886.9	GHO	2.5 × 6.0	5700–7460	11	2.3
43	2003 Oct 17	52929.7	GHO	2.5 × 6.0	4300–6060	10	2.3
44	2003 Oct 18	52930.7	GHO	2.5 × 6.0	5700–7460	11	1.8
45	2003 Oct 20	52932.7	GHO	2.5 × 6.0	3800–7100	12	1.8
46	2003 Nov 19	52962.6	GHO	2.5 × 6.0	4300–6060	10	2.3
47	2003 Nov 20	52963.7	GHO	2.5 × 6.0	5700–7460	12	2.6
48	2003 Dec 17	52990.6	GHO	2.5 × 6.0	4300–6060	9	3.1
49	2003 Dec 18	52991.6	GHO	2.5 × 6.0	5300–7460	12	2.7
50	2003 Dec 20	52993.6	GHO	2.5 × 6.0	3800–7100	15	2.3
51	2004 Aug 17	53234.9	GHO	2.5 × 6.0	3800–7100	15	2.5
52	2004 Aug 18	53235.8	GHO	2.5 × 6.0	4300–6060	9	3.1
53	2004 Aug 19	53236.8	GHO	2.5 × 6.0	5700–7460	12	3.1
54	2004 Aug 20	53237.9	GHO	2.5 × 6.0	3800–7100	15	2.7
55	2004 Sep 5	53253.9	GHO	2.5 × 6.0	3800–7100	15	2.7
56	2004 Sep 6	53254.8	GHO	2.5 × 6.0	4300–6060	8	2.7
57	2004 Sep 8	53256.8	GHO	2.5 × 6.0	5700–7460	10	3.6
58	2004 Nov 12	53321.6	GHO	2.5 × 6.0	3800–7100	14	2.3
59	2004 Nov 17	53326.6	GHO	2.5 × 6.0	4300–6060	11	2.7
60	2004 Nov 18	53327.6	GHO	2.5 × 6.0	3800–7100	14	2.3
61	2004 Dec 13	53352.6	GHO	2.5 × 6.0	3800–7100	12	3.6
62	2004 Dec 14	53353.6	GHO	2.5 × 6.0	4300–6060	7	3.6
63	2004 Dec 15	53354.6	GHO	2.5 × 6.0	5700–7460	8	2.3
64	2005 May 14	53505.0	SPM	2.5 × 6.0	3880–5960	7	4.9

Table 2
(Continued)

No.	UT Date	JD+ 2400000+	CODE	Aperture (arcsec)	Spectral Range (Å)	Resolution (Å)	Seeing (arcsec)
1	2	3	4	5	6	7	8
65	2005 May 15	53506.0	SPM	2.5 × 6.0	5720–7580	7	3.3
66	2005 Aug 26	53608.9	GHO	2.5 × 6.0	3800–7100	13	2.9
67	2005 Aug 27	53609.9	GHO	2.5 × 6.0	4150–7460	12	3.4
68	2005 Aug 28	53610.8	GHO	2.5 × 6.0	4330–6000	7	2.8
69	2005 Aug 29	53611.8	GHO	2.5 × 6.0	4330–6000	8	3.9
70	2005 Aug 30	53612.8	GHO	2.5 × 6.0	4330–6000	8	3.3
71	2005 Aug 31	53613.8	GHO	2.5 × 6.0	4330–6000	7	2.7
72	2005 Sep 8	53621.9	SPM	2.5 × 6.0	3700–5790	10	3.0
73	2005 Sep 9	53622.9	SPM	2.5 × 6.0	3700–5780	8	. . .
74	2005 Sep 28	53641.8	GHO	2.5 × 6.0	4320–5980	7	2.7
75	2005 Sep 29	53642.6	GHO	2.5 × 6.0	5740–7400	8	3.1
76	2005 Sep 30	53643.8	GHO	2.5 × 6.0	4290–5960	7	2.8
77	2005 Oct 24	53667.6	GHO	2.5 × 6.0	3750–7050	12	2.3
78	2005 Oct 26	53669.7	GHO	2.5 × 6.0	4260–5920	8	3.0
79	2005 Oct 28	53671.7	GHO	2.5 × 6.0	5740–7400	8	3.1
80	2005 Nov 28	53702.6	GHO	2.5 × 6.0	3800–6908	14	3.0
81	2005 Nov 29	53703.6	GHO	2.5 × 6.0	4300–5917	8	5.0
82	2005 Nov 30	53704.6	GHO	2.5 × 6.0	5740–7400	8	2.0
83	2005 Dec 5	53710.6	SPM	2.5 × 6.0	3700–5770	7	. . .
84	2005 Dec 7	53711.6	SPM	2.5 × 6.0	3700–5770	7	2.8
85	2005 Dec 29	53733.6	GHO	2.5 × 6.0	4300–6010	10	2.3
86	2006 Jun 28	53915.5	Z2K	4.0 × 4.0	3740–7400	9	2.5
87	2006 Aug 27	53974.9	GHO	2.5 × 6.0	3600–7050	12	2.2
88	2006 Aug 29	53977.5	Z2K	4.0 × 4.0	3750–7400	9	2.0
89	2006 Aug 30	53978.5	Z2K	4.0 × 4.0	3750–7400	8	2.0
90	2006 Aug 30	53977.8	GHO	2.5 × 6.0	4120–5920	8	2.5
91	2006 Aug 31	53978.8	GHO	2.5 × 6.0	3600–7050	12	2.2
92	2006 Sep 15	53993.8	GHO	2.5 × 6.0	3600–7050	13	3.4
93	2006 Sep 17	53995.7	GHO	2.5 × 6.0	3600–7050	13	2.4
94	2006 Sep 18	53996.8	GHO	2.5 × 6.0	4130–5030	7	2.5
95	2006 Sep 19	53997.8	GHO	2.5 × 6.0	3600–7000	12	2.8
96	2006 Sep 28	54006.7	SPM	2.5 × 6.0	3740–5810	7	3.3
97	2006 Sep 29	54007.7	SPM	2.5 × 6.0	3740–5810	7	3.3
98	2006 Oct 23	54031.7	SPM	2.5 × 6.0	3700–5900	8	2.6
99	2006 Oct 27	54035.7	GHO	2.5 × 6.0	3700–7280	12	2.8
100	2006 Oct 28	54036.7	GHO	2.5 × 6.0	4230–6040	8	2.4
101	2006 Oct 30	54038.7	GHO	2.5 × 6.0	3700–7270	14	2.3
102	2006 Oct 31	54039.7	GHO	2.5 × 6.0	4160–5960	8	2.3
103	2006 Nov 30	54069.6	SPM	2.5 × 6.0	3680–7560	12	4.6
104	2007 May 22	54242.9	SPM	2.5 × 6.0	3730–5810	8	3.0
105	2007 May 23	54244.0	SPM	2.5 × 6.0	3730–5810	8	3.2
106	2007 Aug 10	54322.9	GHO	2.5 × 6.0	3870–7430	11	3.0
107	2007 Aug 11	54323.8	GHO	2.5 × 6.0	4340–6140	7	3.2
108	2007 Sep 3	54346.8	GHO	2.5 × 6.0	4330–6130	7	3.6
109	2007 Sep 4	54347.8	GHO	2.5 × 6.0	4150–5950	7	2.6
110	2007 Sep 7	54350.9	GHO	2.5 × 6.0	3860–7420	12	3.0
111	2007 Oct 15	54388.7	GHO	2.5 × 6.0	3870–7440	12	1.8
112	2007 Oct 17	54390.6	GHO	2.5 × 6.0	4190–6000	8	2.5
113	2007 Oct 18	54391.7	GHO	2.5 × 6.0	4190–6000	8	2.2
114	2007 Nov 1	54405.7	GHO	2.5 × 6.0	4190–6000	8	3.0
115	2007 Nov 2	54406.6	GHO	2.5 × 6.0	4190–6000	8	3.3
116	2007 Nov 3	54407.6	GHO	2.5 × 6.0	3820–7390	12	2.9
117	2007 Nov 6	54410.7	GHO	2.5 × 6.0	3830–7400	12	2.4
118	2007 Nov 8	54412.6	GHO	2.5 × 6.0	4290–6100	8	2.4
119	2009 Aug 14	55058.5	Z2K	4.0 × 4.0	3750–7390	8	2.0
120	2009 Oct 11	55116.4	Z2K	4.0 × 4.0	3750–7390	8	1.5

Notes. Column 1: number; Column 2: UT date; Column 3: Julian date (JD); Column 4: code given according to Table 1; Column 5: projected spectrograph entrance apertures; Column 6: wavelength range covered; Column 7: spectral resolution determined from [O III]5007 line and from [O I]6300 when only the red part of the spectrum is present; Column 8: mean seeing in arcsec.

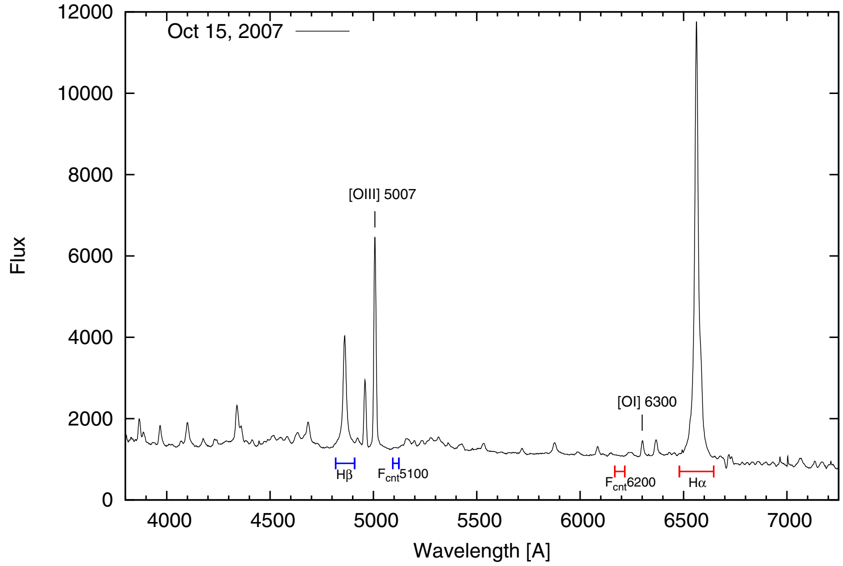

Figure 1. Example of the total optical spectrum of Ark 564. The windows for Hβ, Hα, blue, and red continuum measurements are marked.
(A color version of this figure is available in the online journal.)

Table 3
Flux Scale Factors for Optical Spectra

Sample	Years	Aperture (arcsec)	Scale Factor (φ)	Extended Source Correction $G(g)$[a]
L(U,N)	1999–2010	2.0 × 6.0	1.089	−0.130
GHO	1999–2007	2.5 × 6.0	1.000	0.000
SPM	2005–2007	2.5 × 6.0	1.000	0.000
Z1K	1999–2001	4.0 × 19.8	1.152 ± 0.013	0.998 ± 0.368
Z2K	2005–2007	4.0 × 4.0	0.893 ± 0.052	1.005 ± 0.548
GHO[b]	1999–2007	2.5 × 6.0	1.067 ± 0.048	0.000

Notes.
[a] In units 10^{-15} erg s^{-1} cm^{-2} Å^{-1}.
[b] Resolution 15 Å.

averaging the flux in the spectral interval 6178–6216 Å in the rest frame (Table 5). These interval wavelengths were selected because they do not contain noticeable emission lines (Fe II or any other lines, see Figure 1).

In order to determine the observed fluxes of the Hα, Hβ, and Fe II lines, we need to subtract the underlying continuum; thus, a linear continuum was defined through 20 Å windows located at rest-frame wavelengths 4762 Å (4880 Å in the observed frame) and 5123 Å (5250 Å in the observed frame) for the Hβ line, and at rest-frame wavelengths 6334 Å (6490 Å in the observed frame) and 6656 Å (6820 Å in the observed frame) for the Hα line (Figure 1). In the case of Fe II emission, a precise subtraction of the underlying continuum for a larger wavelength range is required. Hence, a polynomial fit for the continuum was drawn through continuum windows (Figure 2) located at the rest-frame wavelength intervals 4210–4230 Å, 5080–5100 Å, and 5600–5630 Å (see, e.g., Kuraszkiewicz et al. 2002; Kovačević et al. 2010).

After the continuum subtraction, we measured the observed fluxes of the emission lines in the following rest-frame wavelength intervals: 4817–4909 Å for Hβ, 6480–6646 Å for Hα, and 5100–5470 Å for the Fe II emission (hereafter Fe II red shelf). The measurements are given in Table 5. In this Fe II wavelength range, primarily the 48 and 49 Fe II multiplets are located (Figure 2), yet there is also a contribution from the 42 multiplets around 5170 Å in the rest frame (see Kovačević et al. 2010). This spectral interval was chosen because the Fe II lines included there are not blended with other strong broad and narrow emission lines (e.g., He II 4686 Å). This allowed us to determine the Fe II line fluxes in a straightforward manner (Figure 2). Further in the text, we discuss a more detailed analysis of the Fe II emission in a wider spectral interval 4100–5600 Å in the rest frame (see Section 5).

Worth noting is the fact that the Hβ and Hα fluxes reported here include the corresponding narrow component fluxes: In the case of Hβ, only the narrow Hβ is included (the [O III] $\lambda\lambda$4959, 5007 lines are out from the Hβ spectral interval), while for the Hα case, lines of [N II]$\lambda\lambda$6548,6584 and narrow Hα are included. As fluxes of narrow lines are assumed to be constant, they have no influence on the broad-line component variability. The line and continuum fluxes were corrected for the aperture effect using the correction factors listed in Table 3 (see Section 2.2).

In Table 4, the fluxes for the blue continuum (at 5100 Å), Hα, Hβ, and Fe II lines are listed. We have also estimated the flux contribution from the Hβ and Hα narrow components and [N II] $\lambda\lambda$6548, 6584, from multi-Gaussian fit to the blends (Hβ+[O III] $\lambda\lambda$4959, 5007 and Hα+[N II] $\lambda\lambda$6548, 6584) of the mean profiles. The best fits are plotted in Figure 3. From the mean spectra, the estimated contribution of the F(Hβ) narrow component to the total line flux is ∼20%. The narrow F(Hα) has a contribution of about 30%, while the fluxes of the [N II] $\lambda\lambda$6548, 6584 have one of 7%. A similar result (an averaged contribution of ∼18%) was obtained for the F(Hβ) narrow component from the Gaussian fit to every blue spectrum (see Section 5).

Additionally, we measured line-segment fluxes. In doing this, we divided the Hα and Hβ line profiles into three parts: a blue wing, a core, and a red wing. The adopted intervals in wavelength and velocity are listed in Table 5.

The mean uncertainties (error bars) for the fluxes of continuum, Hα and Hβ lines, and their line segments (wings and core) are listed in Table 5. These quantities were estimated from the comparison of the results of spectra obtained within a time interval shorter than 3 days. The details of evaluation techniques

Table 4
The Measured Line and Continuum Fluxes

No.	UT Date	JD+ 2400000+	$F_{cnt} \pm \sigma$ (10^{-15} erg cm^{-2} s^{-1} Å^{-1})	F(Hα)$\pm\sigma$ (10^{-13} erg cm^{-2} s^{-1})	F(Hβ)$\pm\sigma$ (10^{-13} erg cm^{-2} s^{-1})	Fe II$_{5100-5470} \pm \sigma$ (10^{-13} erg cm^{-2} s^{-1})
1	2	3	4	5	6	7
1	1999 Sep 2	51424.4	6.145 ± 0.430	...	2.471 ± 0.082	2.349 ± 0.170
2	1999 Sep 3	51425.4	5.479 ± 0.384	...	2.486 ± 0.082	2.085 ± 0.151
3	1999 Sep 4	51426.4	5.507 ± 0.325	...	2.464 ± 0.081	2.162 ± 0.336
4	1999 Sep 5	51427.3	6.246 ± 0.437	11.963 ± 0.447	2.589 ± 0.085	2.696 ± 0.419
5	1999 Oct 3	51455.2	5.733 ± 0.214	11.119 ± 0.416	2.008 ± 0.221	...
6	1999 Oct 4	51456.2	5.828 ± 0.218	11.707 ± 0.438	2.348 ± 0.258	...
7	1999 Oct 9	51461.3	6.176 ± 0.231	...	2.459 ± 0.081	2.111 ± 0.152
8	1999 Oct 13	51465.2	5.329 ± 0.199	...	2.478 ± 0.082	1.948 ± 0.141
9	1999 Nov 2	51485.3	5.742 ± 0.215	...	2.233 ± 0.074	2.496 ± 0.405
10	1999 Nov 3	51486.2	5.705 ± 0.213	...	2.253 ± 0.074	1.798 ± 0.291
11	1999 Nov 4	51487.2	6.013 ± 0.225	...	2.348 ± 0.077	2.170 ± 0.352
12	1999 Nov 5	51488.2	6.384 ± 0.239	...	2.478 ± 0.082	...
13	1999 Nov 6	51489.2	6.030 ± 0.226	...	2.388 ± 0.079	2.566 ± 0.185
14	1999 Nov 30	51513.2	5.635 ± 0.211	...	2.584 ± 0.085	2.590 ± 0.187
15	1999 Dec 2	51515.2	5.583 ± 0.209	...	2.643 ± 0.087	1.978 ± 0.143
16	2000 May 28	51693.5	5.643 ± 0.211	...	2.447 ± 0.081	2.794 ± 0.202
17	2000 Jun 6	51702.4	5.829 ± 0.218	...	2.822 ± 0.093	2.016 ± 0.146
18	2000 Jul 8	51734.4	5.982 ± 0.431	...	2.578 ± 0.085	2.493 ± 0.394
19	2000 Jul 9	51735.4	5.208 ± 0.375	...	2.745 ± 0.091	1.950 ± 0.308
20	2000 Jul 10	51736.4	5.822 ± 0.419	...	2.836 ± 0.094	2.669 ± 0.422
21	2000 Oct 16	51833.7	5.809 ± 0.217	11.346 ± 0.424	2.500 ± 0.083	2.330 ± 0.168
22	2001 Nov 23	52236.6	5.722 ± 0.214	...	2.630 ± 0.087	2.292 ± 0.168
23	2001 Nov 23	52237.1	5.725 ± 0.214	...	2.629 ± 0.087	2.324 ± 0.166
24	2001 Nov 24	52237.6	...	10.658 ± 0.399	...	...
25	2002 Aug 15	52501.8	4.747 ± 0.178	...	2.472 ± 0.082	1.836 ± 0.133
26	2002 Aug 17	52503.9	...	10.094 ± 0.378	...	...
27	2002 Nov 11	52589.7	5.528 ± 0.207	...	2.760 ± 0.091	2.619 ± 0.189
28	2002 Nov 12	52590.7	...	10.285 ± 0.385	...	...
29	2002 Nov 13	52591.7	...	10.402 ± 0.389	...	...
30	2002 Nov 14	52592.7	5.873 ± 0.220	10.537 ± 0.394	2.790 ± 0.092	2.403 ± 0.173
31	2002 Dec 10	52618.6	5.294 ± 0.198	...	2.782 ± 0.092	2.341 ± 0.169
32	2002 Dec 11	52619.6	...	9.750 ± 0.365	...	...
33	2002 Dec 12	52620.6	5.578 ± 0.209	9.936 ± 0.372	2.607 ± 0.086	2.288 ± 0.165
34	2003 Sep 4	52886.9	...	9.700 ± 0.363	...	...
35	2003 Oct 17	52929.7	5.016 ± 0.188	...	2.460 ± 0.081	1.928 ± 0.139
36	2003 Oct 18	52930.7	...	8.925 ± 0.334	...	...
37	2003 Oct 20	52932.7	4.961 ± 0.186	8.950 ± 0.335	2.398 ± 0.079	1.807 ± 0.130
38	2003 Nov 19	52962.6	4.738 ± 0.177	...	2.420 ± 0.080	1.993 ± 0.144
39	2003 Nov 20	52963.7	...	8.968 ± 0.335	...	...
40	2003 Dec 17	52990.6	6.504 ± 0.748	...	3.070 ± 0.190	2.600 ± 0.264
41	2003 Dec 18	52991.6	...	11.069 ± 0.414	...	...
42	2003 Dec 20	52993.6	5.526 ± 0.636	10.313 ± 0.386	2.813 ± 0.174	2.251 ± 0.229
43	2004 Aug 17	53234.9	5.038 ± 0.589	9.375 ± 0.506	2.429 ± 0.080	1.798 ± 0.235
44	2004 Aug 18	53235.8	6.123 ± 0.716	...	2.566 ± 0.085	2.280 ± 0.298
45	2004 Aug 19	53236.8	...	8.489 ± 0.458	...	...
46	2004 Aug 20	53237.9	5.027 ± 0.588	9.303 ± 0.502	2.405 ± 0.079	1.872 ± 0.245
47	2004 Sep 5	53253.9	5.325 ± 0.405	10.132 ± 0.598	2.501 ± 0.208	1.812 ± 0.131
48	2004 Sep 6	53254.8	4.781 ± 0.363	...	2.225 ± 0.185	1.793 ± 0.129
49	2004 Sep 8	53256.8	...	9.327 ± 0.550	...	...
50	2004 Nov 12	53321.6	5.046 ± 0.189	9.504 ± 0.355	2.548 ± 0.084	1.964 ± 0.142
51	2004 Nov 17	53326.6	5.369 ± 0.201	...	2.687 ± 0.089	...
52	2004 Nov 18	53327.6	5.085 ± 0.190	9.862 ± 0.369	2.508 ± 0.083	1.909 ± 0.138
53	2004 Dec 13	53352.6	6.088 ± 0.228	11.049 ± 0.413	2.787 ± 0.092	2.350 ± 0.170
54	2004 Dec 14	53353.6	5.814 ± 0.217	...	2.657 ± 0.088	2.596 ± 0.187
55	2004 Dec 15	53354.6	...	10.268 ± 0.384	...	...
56	2005 May 14	53505.0	4.954 ± 0.185	...	2.091 ± 0.069	1.918 ± 0.138
57	2005 May 14	53506.0	...	10.081 ± 0.377	...	...
58	2005 Aug 26	53608.9	4.448 ± 0.166	8.321 ± 0.691	2.283 ± 0.075	1.919 ± 0.139
59	2005 Aug 27	53609.9	4.937 ± 0.185	9.362 ± 0.777	2.450 ± 0.081	1.724 ± 0.125
60	2005 Aug 28	53610.8	4.559 ± 0.170	...	2.310 ± 0.076	1.988 ± 0.144
61	2005 Aug 29	53611.8	4.678 ± 0.175	...	2.360 ± 0.078	1.880 ± 0.136
62	2005 Aug 30	53612.8	4.593 ± 0.172	...	2.268 ± 0.075	2.035 ± 0.147
63	2005 Aug 31	53613.8	4.704 ± 0.176	...	2.289 ± 0.076	2.160 ± 0.156
64	2005 Sep 8	53621.9	4.498 ± 0.168	...	2.118 ± 0.070	1.543 ± 0.238

Table 4
(Continued)

No.	UT Date	JD+ 2400000+	$F_{cnt} \pm \sigma$ (10^{-15} erg cm^{-2} s^{-1} Å^{-1})	F(Hα)$\pm\sigma$ (10^{-13} erg cm^{-2} s^{-1})	F(Hβ)$\pm\sigma$ (10^{-13} erg cm^{-2} s^{-1})	Fe II$_{5100-5470} \pm \sigma$ (10^{-13} erg cm^{-2} s^{-1})
1	2	3	4	5	6	7
65	2005 Sep 9	53622.9	4.809 ± 0.180	...	2.128 ± 0.070	1.921 ± 0.296
66	2005 Sep 28	53641.8	4.333 ± 0.162	...	2.270 ± 0.075	1.708 ± 0.123
67	2005 Sep 29	53642.6	...	8.359 ± 0.313	...	...
68	2005 Sep 30	53643.8	4.378 ± 0.164	...	2.182 ± 0.072	1.838 ± 0.133
69	2005 Oct 24	53667.6	4.556 ± 0.170	9.429 ± 0.353	2.133 ± 0.070	1.908 ± 0.138
70	2005 Oct 26	53669.7	4.457 ± 0.167	...	2.176 ± 0.072	1.806 ± 0.130
71	2005 Oct 28	53671.7	...	9.112 ± 0.341	...	...
72	2005 Nov 28	53702.6	4.072 ± 0.470	...	1.982 ± 0.239	1.628 ± 0.321
73	2005 Nov 29	53703.6	4.736 ± 0.470	...	2.320 ± 0.239	2.156 ± 0.425
74	2005 Nov 30	53704.6	...	9.397 ± 0.351	...	...
75	2005 Dec 5	53710.6	4.714 ± 0.176	...	2.267 ± 0.075	1.761 ± 0.127
76	2005 Dec 7	53711.6	4.507 ± 0.169	...	2.146 ± 0.071	1.714 ± 0.124
77	2005 Dec 29	53733.6	4.475 ± 0.167	...	2.270 ± 0.075	1.834 ± 0.132
78	2006 Aug 27	53974.9	4.538 ± 0.286	9.399 ± 0.352	2.384 ± 0.079	1.942 ± 0.140
79	2006 Aug 29	53977.5	...	9.254 ± 0.346	...	...
80	2006 Aug 30	53977.8	4.642 ± 0.174	...	2.335 ± 0.077	1.774 ± 0.128
81	2006 Aug 30	53978.5	...	8.801 ± 0.329	...	...
82	2006 Aug 31	53978.8	4.558 ± 0.170	9.337 ± 0.349	2.273 ± 0.075	1.877 ± 0.135
83	2006 Sep 15	53993.8	4.953 ± 0.185	9.883 ± 0.370	2.511 ± 0.083	1.959 ± 0.141
84	2006 Sep 17	53995.7	4.889 ± 0.183	9.941 ± 0.372	2.469 ± 0.081	2.068 ± 0.149
85	2006 Sep 18	53996.8	4.899 ± 0.183	...	2.288 ± 0.076	1.686 ± 0.122
86	2006 Sep 19	53997.8	4.626 ± 0.173	9.352 ± 0.350	2.352 ± 0.078	1.916 ± 0.138
87	2006 Sep 28	54006.7	4.501 ± 0.168	...	2.156 ± 0.071	2.011 ± 0.145
88	2006 Sep 29	54007.7	4.625 ± 0.173	...	2.200 ± 0.073	1.951 ± 0.141
89	2006 Oct 23	54031.7	4.819 ± 0.180	...	1.910 ± 0.063	2.101 ± 0.152
90	2006 Oct 27	54035.7	4.643 ± 0.174	9.319 ± 0.349	2.305 ± 0.076	1.916 ± 0.317
91	2006 Oct 28	54036.7	4.570 ± 0.171	...	2.280 ± 0.075	1.515 ± 0.250
92	2006 Oct 30	54038.7	4.781 ± 0.320	9.930 ± 0.371	2.434 ± 0.153	1.840 ± 0.133
93	2006 Oct 31	54039.7	4.348 ± 0.291	...	2.225 ± 0.141	1.810 ± 0.131
94	2006 Nov 30	54069.6	4.922 ± 0.184	9.999 ± 0.374	2.240 ± 0.074	1.959 ± 0.141
95	2007 May 22	54242.9	4.702 ± 0.176	...	2.285 ± 0.075	1.919 ± 0.139
96	2007 May 23	54244.0	4.707 ± 0.176	...	2.209 ± 0.073	1.839 ± 0.133
97	2007 Aug 10	54322.9	4.683 ± 0.175	8.973 ± 0.336	2.398 ± 0.079	1.907 ± 0.138
98	2007 Aug 11	54323.8	4.667 ± 0.175	...	2.422 ± 0.080	1.927 ± 0.139
99	2007 Sep 3	54346.8	4.668 ± 0.175	...	2.491 ± 0.082	1.758 ± 0.177
100	2007 Sep 4	54347.8	4.696 ± 0.176	...	2.385 ± 0.079	2.027 ± 0.204
101	2007 Sep 7	54350.9	4.430 ± 0.166	9.760 ± 0.365	2.496 ± 0.082	1.715 ± 0.124
102	2007 Oct 15	54388.7	4.318 ± 0.161	9.360 ± 0.350	2.306 ± 0.076	1.834 ± 0.132
103	2007 Oct 17	54390.6	4.446 ± 0.166	...	2.401 ± 0.079	1.969 ± 0.142
104	2007 Oct 18	54391.7	4.344 ± 0.162	...	2.396 ± 0.079	1.874 ± 0.135
105	2007 Nov 1	54405.7	4.413 ± 0.165	...	2.403 ± 0.079	2.033 ± 0.147
106	2007 Nov 2	54406.6	4.399 ± 0.165	...	2.472 ± 0.082	1.871 ± 0.135
107	2007 Nov 3	54407.6	4.594 ± 0.172	9.530 ± 0.356	2.444 ± 0.081	1.964 ± 0.142
108	2007 Oct 6	54410.7	4.367 ± 0.163	9.973 ± 0.373	2.414 ± 0.080	1.870 ± 0.135
109	2007 Nov 8	54412.6	4.287 ± 0.160	...	2.332 ± 0.077	2.002 ± 0.145
110	2009 Aug 14	55058.5	...	10.712 ± 0.401	...	...
111	2009 Oct 11	55116.4	...	12.204 ± 0.456	...	...

of these uncertainties (error bars) are given in Shapovalova et al. (2008). As can be seen in Table 5, the mean error of the continuum flux, total Hα and Hβ lines, and their cores is ∼4%. Due to their relatively weaker flux, the errors in the determination of the fluxes of the Fe II and line wings are larger, about ∼7%–9%.

3. RESULTS OF THE DATA ANALYSIS

3.1. *Variability of the Emission Lines and of the Optical Continuum*

We analyzed flux variations in the continuum and emission lines from a total of 91 spectra covering the Hβ wavelength region, and 50 spectra covering the Hα line vicinity. In Figure 4, the blue continuum-subtracted spectrum of Ark 564, obtained with the 6 m SAO telescope on 2001 November 23 (JD 2452237.1), is presented. There, we mark the positions of some relevant Fe II multiplets (27, 28, 37, 38, 42, 48, and 49) and other important emission lines. As can easily be seen, the Fe II emission is rather strong, as is usually the case in NLS1 galaxies.

From the flux data listed in Table 4, we obtained light curves for the blue and red continua and for Hα, Hβ, Fe II emission (Figure 5), and their line segments (blue wing, core, and red wing, see Figure 6). As one can see in Figures 5 and 6, the fluxes declined slowly from the beginning to the end of the monitoring period. For Hα and Hβ a decline of ∼20% is present, while

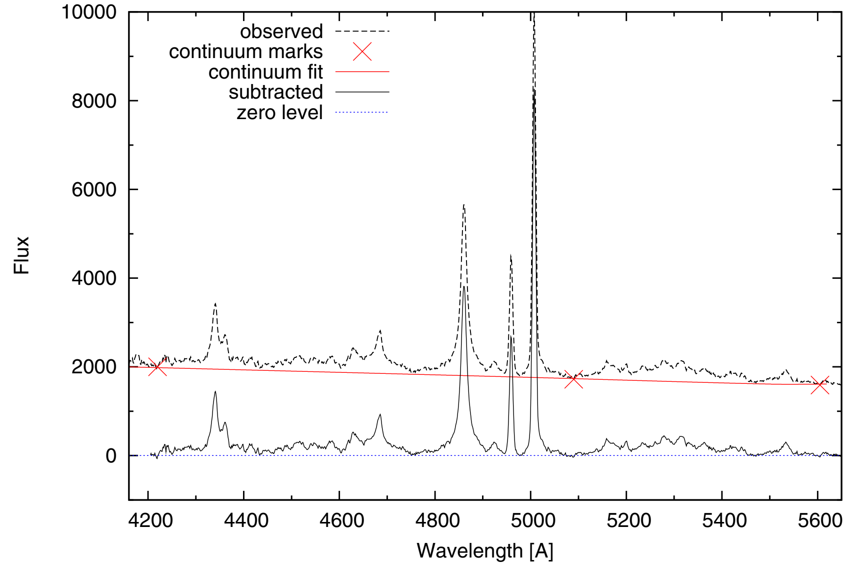

Figure 2. Underlying continuum subtraction in the Hβ region needed for accurate Fe II measurements.
(A color version of this figure is available in the online journal.)

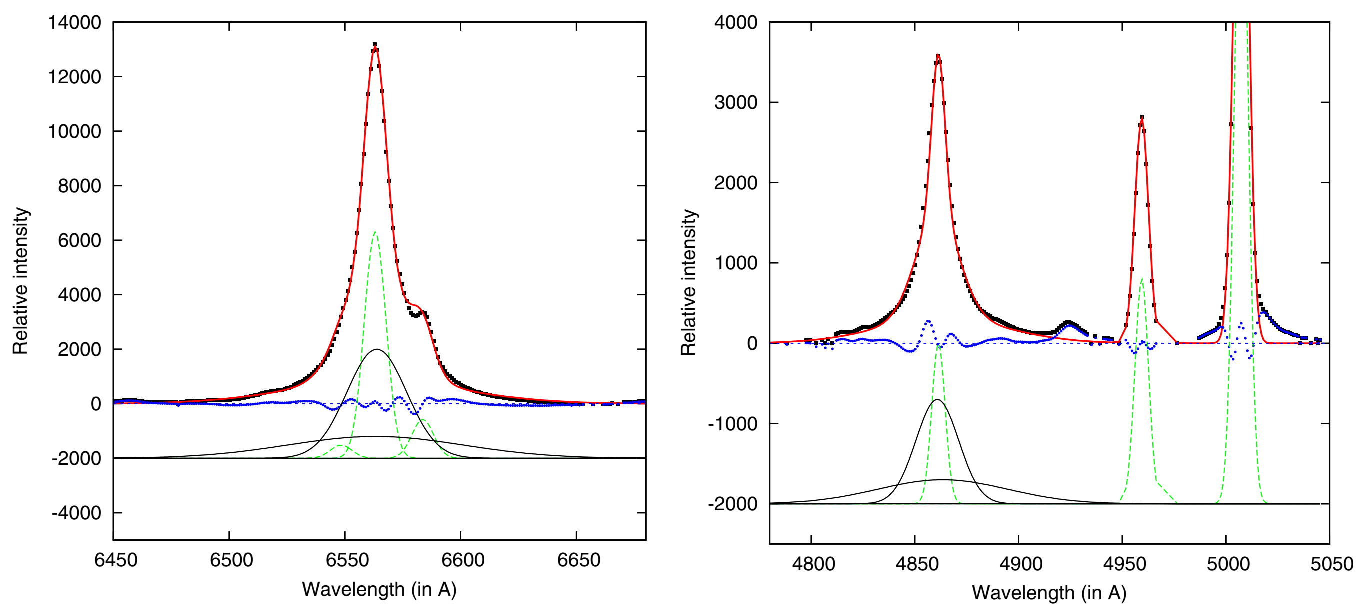

Figure 3. Best Gaussian fitting (solid line) of the mean Hα (left) and Hβ (right) line profiles (dotted line) with a sum of Gaussians. The broad components are fitted with two Gaussians (solid lines) and the narrow lines with one (dashed lines). The line residuals are also given below the observed spectra. In the region of the Hβ the Fe II contribution is not subtracted.

(A color version of this figure is available in the online journal.)

for the Fe II emission a decline of ∼30% and for the continuum flux a decline of ∼40% are seen (Figure 5). In the upper panel of Figure 5, the upper dashed line represents the flux at the beginning of the monitoring campaign, and the lower dashed line that at the end of it. There is only one red point in 2010, at which the red flux increased (two lower panels in Figure 5). Similar to Collier et al. (2001), the light curves show several flare-like increments (see Figure 5). The light curves of line wings and the core (Figure 6) show practically simultaneous variations. There might be up to five flare-like events detected in our data (see Table 6) when the flux increases ∼10%–20% for a short period of time (∼1–3 days, see Table 6), out of which two flares were prominent in 2003 December and 2004 August. As can be seen in Table 6, as a rule, flare-like events in the continuum (see dF(cnt) in %) are stronger than those in emission lines.

Long-term flux-monitoring programs have shown that the flux variations of AGNs tend to be stochastic (i.e., there are few cases of periodicity or quasi-periodicity, see, e.g., Shapovalova et al. 2010). However, the AGN light curves sometimes, as in the case of Ark 564, can show flare-like characteristics whose spectral properties are consistent with a shot-noise process (Cruise & Dodds 1985; Hufnagel & Bregman 1992; Hughes et al. 1992). One way to reproduce shot noise is through a superposition of a series of identical impulses occurring at intervals dictated by Poisson statistics. In a Poisson process, the overall rate of events

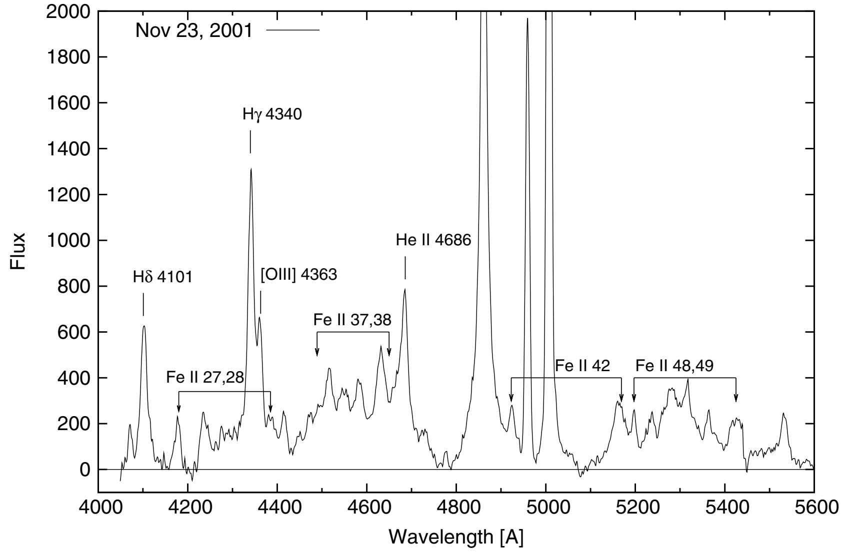

Figure 4. Fe ii emission around the Hβ line for Ark 564.

Table 5
Estimates of the Errors for Line and Line-Segment Fluxes

Line	Spectral Region (Å) (obs)	(Å) (rest)	$\sigma \pm e$ (%)	V_r region (km s^{-1})
cont 5100	5220–5250	5094–5123	3.7 ± 3.3	...
cont 6200	6320–6370	6168–6216	4.5 ± 2.2	...
Hα-total	6640–6810	6480–6646	3.7 ± 2.2	(−3792;+3792)
Hβ-total	4936–5030	4817–4909	3.3 ± 2.5	(−2710;+2950)
Fe ii	5226–5605	5100–5470	7.2 ± 5.6	...
Hα-blue	6635–6698	6475–6537	6.8 ± 6.6	(−4015;−1204)
Hα-core	6698–6752	6537–6589	3.5 ± 2.1	(−1204;+1204)
Hα-red	6752–6816	6589–6652	5.6 ± 4.0	(+1204;+4015)
Hβ-blue	4928–4960	4809–4840	8.0 ± 4.9	(−3200;−1200)
Hβ-core	4960–5001	4840–4880	3.0 ± 2.9	(−1200;+1200)
Hβ-red	5001–5034	4880–4913	8.7 ± 5.3	(+1200;+3200)

is statistically constant, yet the starting times of individual events are independent of all previous ones. The time intervals between events follow an exponential distribution. It is possible to use such a process in Ark 564 variability investigation by assuming a constant flare rate ρ and letting Tj be the occurrence time of the jth flare. The probability of no occurrence of a flare in the interval $[Tj, Tj+\tau]$ is $\exp(-\rho\tau)$.

The probability that a second flare will occur within time τ after the first one is $p(\tau) = 1 - \exp(-\rho\tau)$. Actually, we can say that $p[Tn+1-Tn < \tau | T0, T1, \ldots Tn] = 1 - \exp(-\rho\tau)$ means that at least one flare does occur between Tn and $Tn+\tau$.

As can be seen from Table 6, in the continuum and Hβ we have four events in four separate years, which gives a density of events of 0.4 events per year in a 10 year monitoring period. In such a way, we could estimate the probability of time between flare events (which could be recorded in the continuum flux and Hβ line) as $p(\tau) = 1 - \exp(-0.4\tau)$. As for H$\alpha$, we have three events in three separate years over a 10 year period, which leads to $p(\tau) = 1 - \exp(-0.3\tau)$. Finally, in the case of the Fe ii line we have five events in four separate years (two events occurred at the end of 2006 October), so we could take $\rho = 3/10+2/10 = 1/2$, which leads to $p(\tau) = 1 - \exp(-0.5\tau)$. The exponential density is monotonically decreasing; hence, there is a high probability of a short interval and a small probability of a long interval between flares. This means that typically we will have flares occurring close to each other and spaced out by long rare intervals with no occurrence of flares.

In Table 7, we list several parameters characterizing the variability of the continuum, total line, and line-segment fluxes. There are several methods to estimate variability; here we will use the method given by O'Brien et al. (1998). In this method, F denotes the mean flux over the whole observing period and $\sigma(F)$ is its standard deviation. R(max/min) is the ratio of the maximal to minimal fluxes in the monitoring period. F(var) is an inferred (uncertainty-corrected) estimate of the variation amplitude with respect to the mean flux, defined as

$$F(\mathrm{var}) = [\sqrt{\sigma(F)^2 - e^2}]/F(\mathrm{mean}),$$

with e^2 being the mean square value of the individual measurement uncertainty for N observations, i.e., $e^2 = \frac{1}{N}\sum_i^N e(i)^2$ (O'Brien et al. 1998).

From Table 7, one can see that the amplitude of variability F(var) is ∼10% for the continuum and Fe ii emission and ∼7.5% for the total Hβ flux. The Hβ blue wing shows slightly greater variability (F(var) ∼ 15%) than the red one (F(var) ∼ 11%, see Table 7). However, the Hα line wings and core show lower amplitude variability (F(var) ∼ 8%) than the Hβ wings (F(var) ∼ 11%–15%).

3.2. Mean and Root-Mean-Square Spectra

We calculated the mean Hα and Hβ line profiles and their root-mean-square (rms) profiles. To find the different portion of variability in different line parts, as much as it is possible, we first inspect the spectra and conclude that the spectra with spectral resolution ⩽11 Å for Hα and ⩽10 Å for Hβ are good enough for this purpose. Thus, we have a sample of 23 red spectra and 61 blue spectra (Figure 7). For this purpose the spectra were calibrated to have the same spectral resolution (11 Å for Hα and 10 Å for Hβ).

Figure 7 shows that the Hα and Hβ line profiles in Ark 564 are Lorentzian-like (with broad wings), which is a characteristic of the NLS1 galaxies (see, e.g., Sulentic et al. 2009, 2011). The rms profile of Hβ resembles a Lorentzian one, while in the case of Hα there is practically no change in the profile. The FWHM of the Hβ line from the observed mean and rms profiles is 960 km s^{-1},

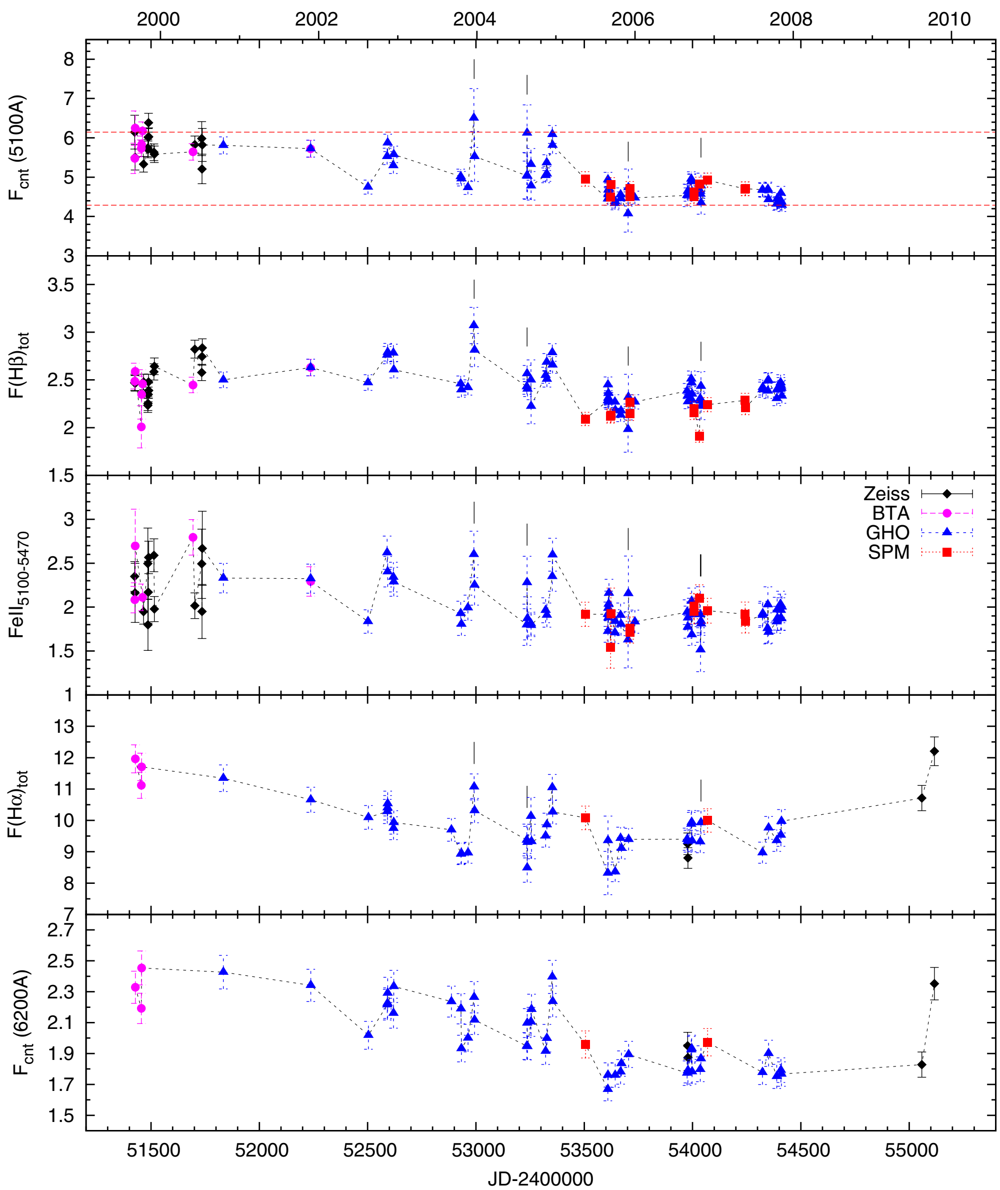

Figure 5. Light curves (from top to bottom) of the continuum at 5100 Å, Hβ, Fe II, Hα, and the continuum at 6200 Å. Data obtained with different telescopes are marked with different symbols: diamonds, 6 m BTA; circles, 1 m Zeiss; triangles, 2.1 m GHO; squares, 2.1 m SPM. The flares are marked on the upper four plots (see Table 6); in the blue continuum plot (first upper plot) the dashed lines represent the first and last observed continuum fluxes to show the decrease of the continuum flux during the monitoring campaign. Continuum fluxes are given in units 10^{-15} erg cm^{-2} s^{-1} Å^{-1} and line fluxes in 10^{-13} erg cm^{-2} s^{-1}.

(A color version of this figure is available in the online journal.)

and from the observed mean profile of Hα is 800 km s^{-1}. The full width at zero intensity (FW0I) of Hβ is much more difficult to measure since the Fe II emission contributes to the red wing. Thus, we only give estimates of FW0I of Hβ mean profiles (or rms) to be ∼8000; for Hα it is also ∼8000 km s^{-1}. As can be seen in Figure 7, the rms is relatively weak ($F_{\rm rms}({\rm H}\alpha)/F_{{\rm H}\alpha} \sim 0.01$ and $F_{\rm rms}({\rm H}\beta)/F_{{\rm H}\beta} \sim 0.07$), meaning that there are no significant changes in the line profiles of Hα and Hβ during the monitoring period. Note here that we re-calibrated the Hβ line, taking the fact that the [O III] lines have the same profile during the monitoring period; therefore, we have small rms in forbidden lines. It is also interesting that the rms shape of Hβ is practically the same as the total Hβ (composed from the broad and narrow components, see Figure 3). This may indicate that the whole (Lorentzian-like) line is emitted from a complex broad-line region (BLR) and that the contribution of the narrow component that is coming from the same region as the [O III] lines is negligible. On the other hand, the Hα line rms shows that the variability is caused mainly by variations in the line wings.

4. THE CONTINUUM VERSUS LINE FLUX CORRELATIONS

To determine whether there are any changes in the structure of the BLR, we investigated both the relationships between the total line fluxes of Hα, Hβ, and Fe II, and between the different line segments (wings and core) of Hα and Hβ.

In Figure 8 the correlation between the total line fluxes of Hβ, Hα, and Fe II are presented. It is interesting to note that

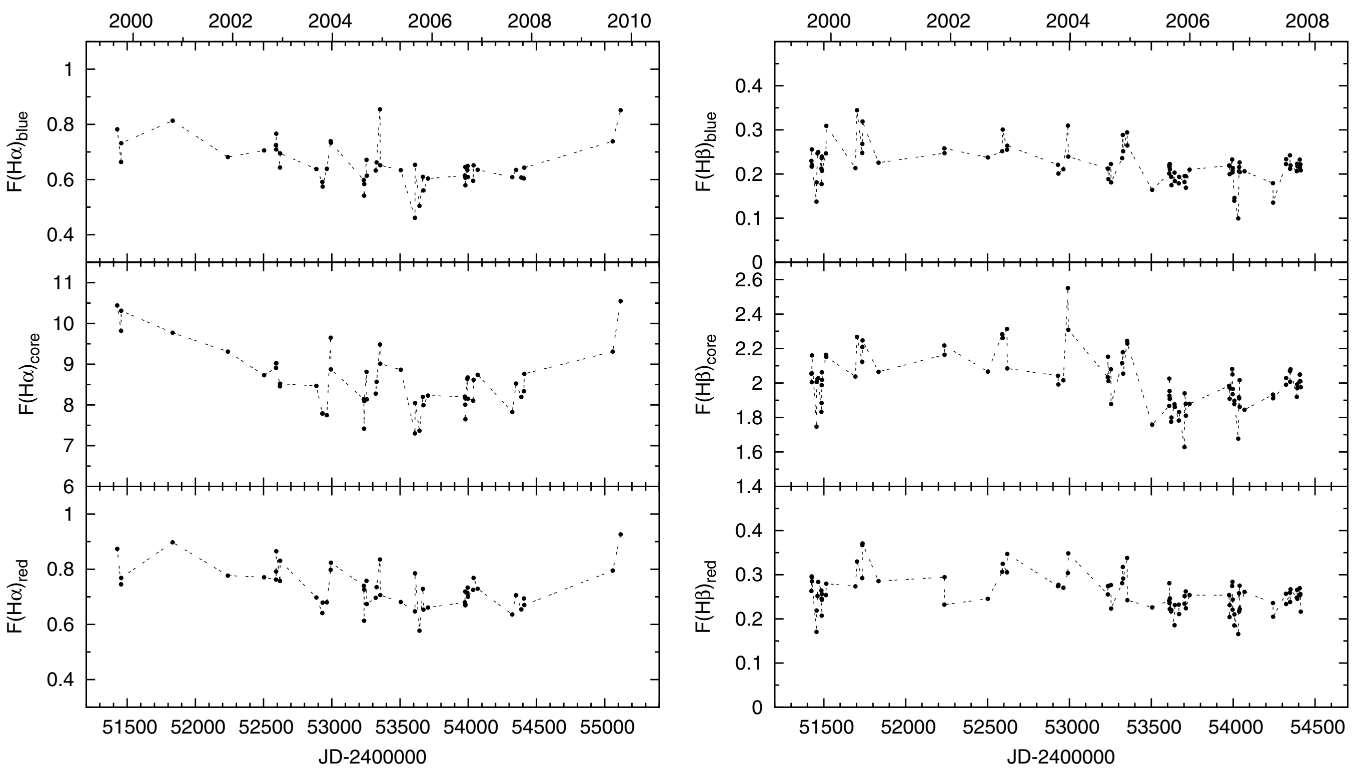

Figure 6. Light curves of the Hα (left) and Hβ (right) line segments (from top to bottom: blue, core, and red line parts).

Table 6
Flares in the Light Curves of the Blue Continuum, Hβ, Hα, and Fe II Emission

No.	Date	JD+ 2400000	F(cnt)[a] (5235)Å	dF(cnt) (%)	F(Hβ)[b]	dF(Hβ) (%)	F(Hα)[b]	dF(Hα) (%)	F(Fe II)[b]	dF(Fe II) (%)
1	2003 Dec 17	52990.6	6.5038	18%	3.070	9%	11.069	7%	2.600	10%
	2003 Dec 20	52993.6	5.5264		2.813		10.313		2.251	
2	2004 Aug 17	53234.9	5.0378	22%	2.429	6%	9.375	10%	1.798	13%
	2004 Aug 18	53235.8	6.1232		2.566		8.489		2.280	
	2004 Aug 20	53237.9	5.0271		2.405		9.303		1.872	
3	2005 Nov 28	53702.6	4.0724	16%	1.982	17%	...	...	1.628	20%
	2005 Nov 29	53703.6	4.7362		2.320		...		2.156	
4	2006 Oct 27	54035.7							1.916	17%
	2006 Oct 28	54036.7							1.515	
5	2006 Oct 30	54038.7	4.7813	10%	2.434	9%	9.319	7%	1.840	7%
	2006 Oct 31	54039.7	4.3478		2.225		9.930		1.810	

Notes.
[a] Continuum flux is in units 10^{-15} erg cm^{-2} s^{-1} A^{-1}.
[b] Line fluxes are in units 10^{-13}erg cm^{-2} s^{-1}.

the correlations between the flux variation of Hβ and Hα is significantly weaker ($r \sim 0.40$, and it seems statistically insignificant with $P = 0.0053$) than that with the Fe II ($r \sim 0.58$ and $P < 10^{-8}$). The lack of correlations between the Hα and Hβ fluxes may indicate a very complex BLR structure. On the other hand, the correlation between different line-segment fluxes (i.e., blue-/red-wing–core, blue-wing–red-wing) are better, especially for Hα (Figure 9).

In Figure 10, we present the relationships between the continuum flux at 6200 Å (for Hα) and 5100 Å (for Hβ) and the total line and line-segment fluxes for Hα and Hβ. As can be seen in Figure 10, the correlation between line and continuum fluxes is weak. Such weak linear correlations of the lines with continuum may indicate the existence of different sources of ionization (AGN source—photoionization, shock-impact excitation, etc.). It is interesting to note that the Fe II emission seems to show a slightly better correlation with the continuum at 5100 Å ($r \sim 0.76$ and $P < 10^{-16}$) than do Balmer lines (Figure 11).

4.1. Balmer Decrement

We have calculated the BD $= F(\text{H}\alpha)/F(\text{H}\beta)$ flux ratio, i.e., the Balmer decrement (see Figure 12), using ∼50 blue and red spectra taken on the same night (or one night before or after). We obtained a mean Balmer decrement value,

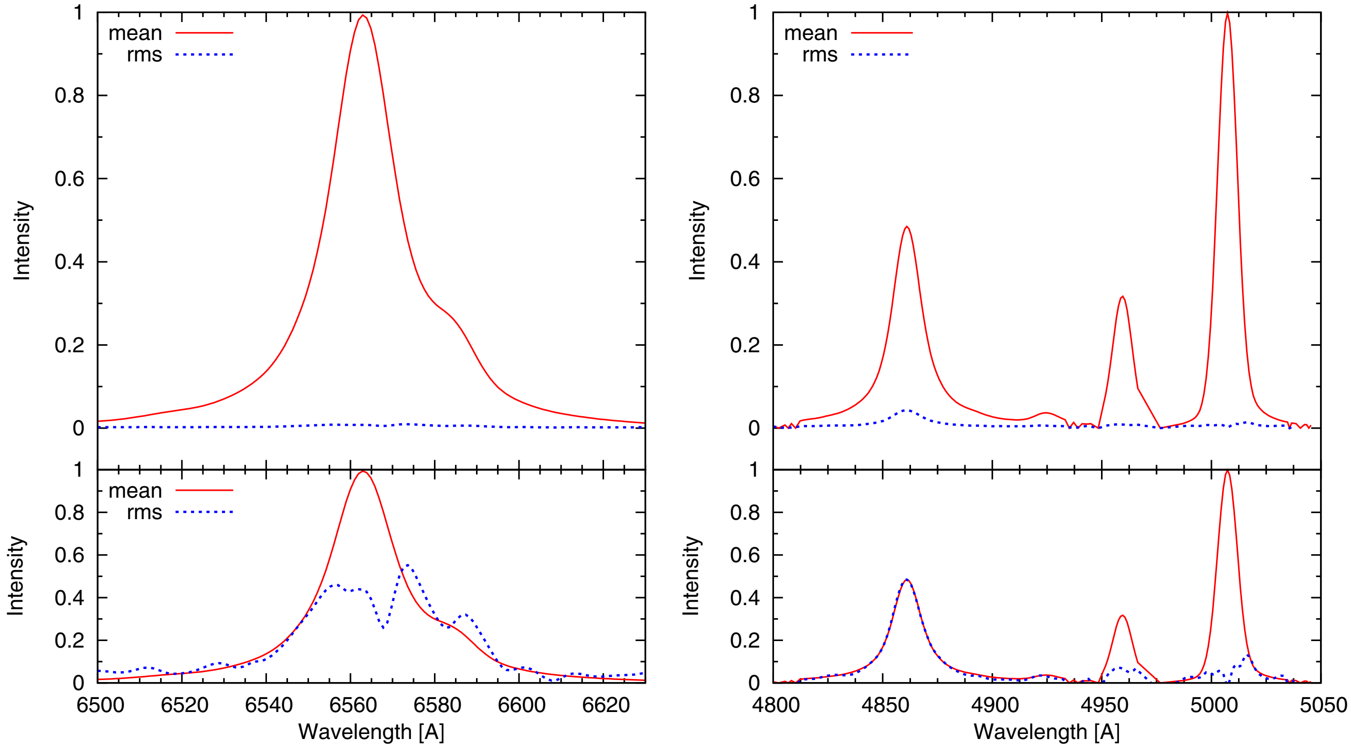

Figure 7. Mean and rms spectra of Hα (left) and Hβ (right) after calibrating the spectra to the same spectral resolution. Bottom plots show the normalized mean and rms spectra arbitrarily scaled for comparison.

(A color version of this figure is available in the online journal.)

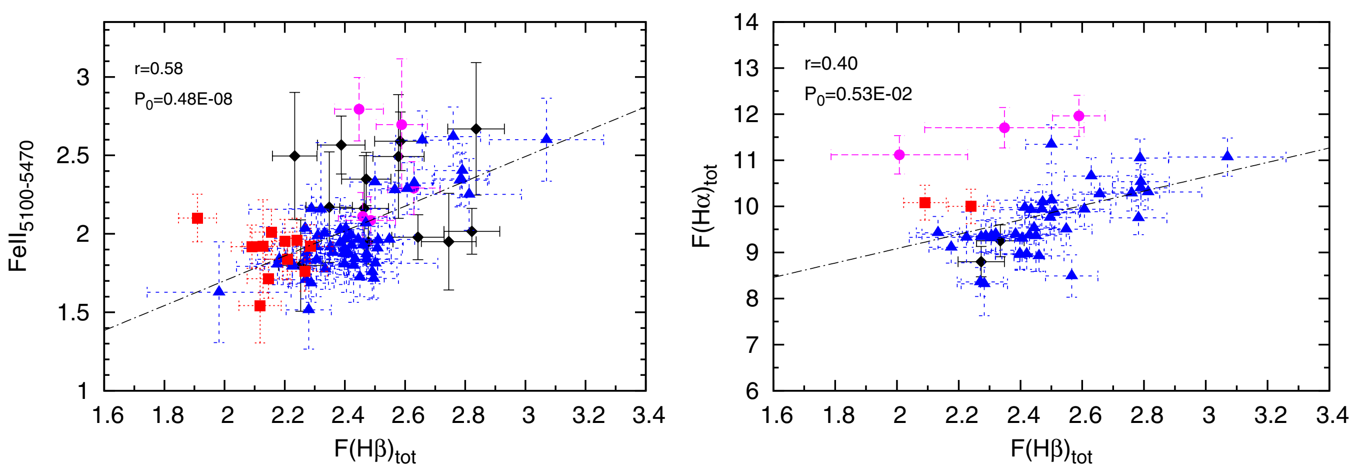

Figure 8. Fe II red shelf (left) and Hα (right) line fluxes as a function of the Hβ line flux. The correlation coefficient and the corresponding *P*-value are given in the upper left corner. The notation is the same as that in Figure 5.

(A color version of this figure is available in the online journal.)

BD (mean) = 4.396 $\pm$ 0.369, and no significant changes in the monitoring period. Figure 12 shows the BD against the continuum flux, and it can be seen that there is no correlation between the BD and the continuum ($R \sim 0.02$). It is apparent that the BD was more or less constant during the 11 year monitoring period. The ratio of Hα and Hβ depends on the physics in the BLR and in the low-density regime; the Hα/Hβ ratio is expected to be below 4, and it has a slight dependence on temperature (see discussion and Figures 6 and 7 in Ilić et al. 2012). In the high-density regime, the Hα/Hβ ratio starts to depend on temperature (see Ilić et al. 2012). The obtained mean BD for Ark 564 seems to be close to the high-density regime, and changes in the BD from 3.5 to 5.5 might be caused by an inhomogeneous BLR; this may indicate a stratified BLR in density, temperature, and rate of ionization.

4.2. Lags between Continuum and Permitted Lines

In order to determine potential time lags between the continuum and permitted line changes, we calculated the cross-correlation function (CCF) for the continuum light curve with the emission-line light curves. There are several ways to construct a CCF, and it is always advisable to use two or more methods to confirm the obtained results. Therefore, we cross-correlated the 5100 Å continuum light curve with both the Hβ and Hα lines (and Fe II emission) light curves using two methods: (1) the *z*-transformed discrete correlation function (ZDCF)

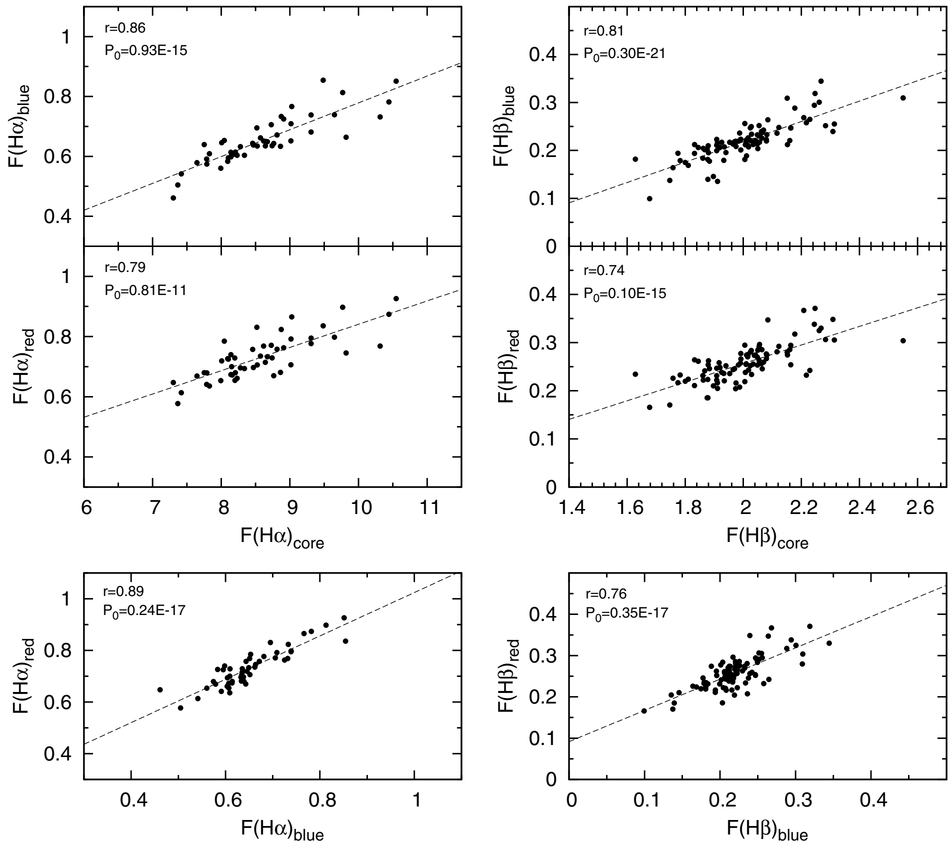

Figure 9. Hα and Hβ line-wing fluxes (blue, red) vs. line-core flux (upper panels), and red vs. blue wing (bottom panels). The correlation coefficient and the corresponding *P*-value are given in the upper left corner.

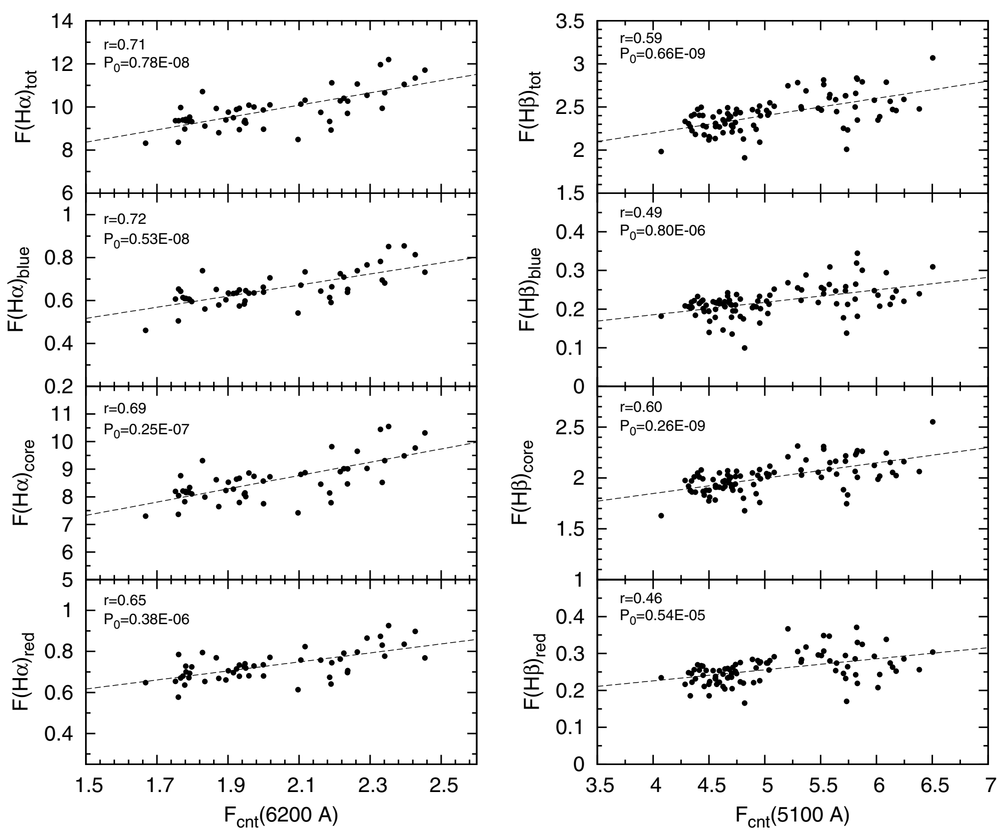

Figure 10. Hα and Hβ lines and line-segment fluxes (blue, core, and red) vs. continuum flux at 6200 and 5100 Å, respectively. The correlation coefficient and the corresponding *P*-value are given in the upper left corner.

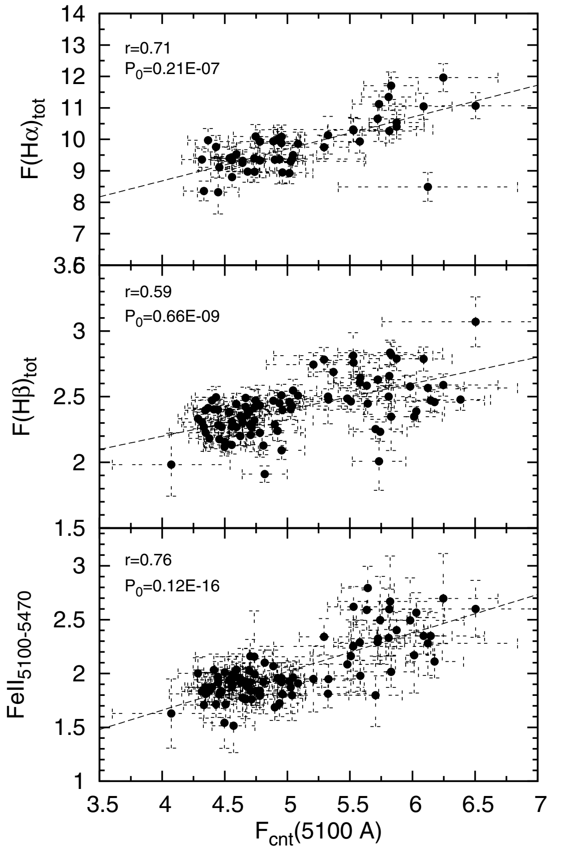

Figure 11. Hα (upper), Hβ (middle), and Fe II (bottom) emission against the continuum flux at 5100 Å. The correlation coefficient and the corresponding *P*-value are given in the upper left corner.

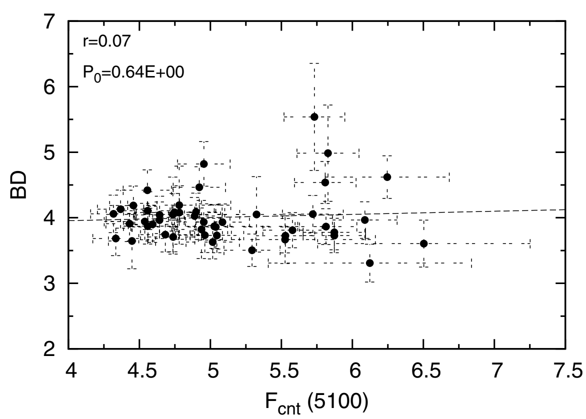

Figure 12. Balmer decrement vs. continuum flux at 5100 Å. The correlation coefficient and the corresponding *P*-value are given in the upper left corner.

method introduced by Alexander (1997) and (2) the interpolation cross-correlation function method (ICCF) described by Bischoff & Kollatschny (1999).

The time lags calculated by ZDCF are given in Table 8, where it can be seen that inferred lags have large associated errors. It is interesting to note that the Fe II lines tend to have shorter lag values, while the longest one is that of the Hα line. If one takes a direct conversion from the time lag to the BLR size, the expected BLR sizes are of an order of 10^{-3} pc (0.003 to 0.0055 pc). This indicates a compact BLR but also a strong stratification in the emitting region of Ark 564, where the Fe II emitting region tends to be very compact and the largest one is the Hα emitting line

Table 7
Parameters of the Continuum and Line Variabilities

Feature	No.	Region (Å)	F(mean)[a]	$\sigma(F)$[a]	R(max/min)	F(var)
1	2	3	4	5	6	7
Continuum 5100	91	5094–5123	5.068	0.608	1.597	0.107
Continuum 6200	50	6168–6216	2.021	0.218	1.471	0.098
Hα-total	50	6480–6646	9.856	0.878	1.467	0.079
Hβ-total	91	4817–4909	2.413	0.206	1.607	0.075
Fe II	87	5100–5470	2.029	0.280	1.844	0.096
Hα-blue	50	6475–6537	0.652	0.079	1.852	0.081
Hα-core	50	6537–6589	8.581	0.757	1.445	0.080
Hα-red	50	6589–6652	0.731	0.074	1.605	0.077
Hβ-blue	91	4809–4840	0.220	0.040	3.465	0.149
Hβ-core	91	4840–4880	2.008	0.152	1.566	0.064
Hβ-red	91	4880–4913	0.258	0.040	2.238	0.110

Notes. Column 1: analyzed feature of the spectrum; Column 2: total number of spectra; Column 3: wavelength region (in the rest frame); Column 4: mean flux[a]; Column 5: standard deviation[a]; Column 6: ratio of the maximal to minimal flux; Column 7: variation amplitude (see the text).
[a] Continuum flux is in units 10^{-15} erg cm^{-2} s^{-1} A^{-1}, and line fluxes and line-segment fluxes are in 10^{-13} erg cm^{-2} s^{-1}.

Table 8
Lags and CCF between the Continuum and Lines

LC1–LC2	Lag (days)	CCF
cnt–Hβ_{tot}	$3.56^{+27.44}_{3.56}$	$0.49^{+0.08}_{-0.09}$
cnt–Fe II	$0.02^{+2.02}_{2.08}$	$0.52^{+0.08}_{-0.08}$
cnt–Hα_{tot}	$4.54^{+5.54}_{14.46}$	$0.49^{+0.01}_{-0.01}$

region. We also calculated the lags using the ICCF and found a delay of ∼6.7 days between the continuum and Hβ line, and of about 0 days between the continuum and Fe II emission, which is in agreement with the ZDCF method (see Table 8). The errors are around 10 lt-day.

The uncertainties in the delays inferred from the CCFs are difficult to estimate, especially the evaluation of a realistic error of the CCF. In our case, the main problem in the time delay determination likely comes from the small variation detected in lines and continuum fluxes (see Table 7) and also their weak correlations (see Figures 10 and 11). Therefore, all obtained lag times should be taken with caution.

5. VARIATION OF THE Fe II LINES

As mentioned above, strong Fe II emission is one of the main characteristics of NLS1 galaxies. Optical Fe II ($\lambda\lambda$4400–5400) emission is one of the most interesting features in AGN spectra. The emission arises from numerous transitions of the complex Fe II ion (see Kovačević et al. 2010, for more details). Iron emission is seen in almost all type-1 AGN spectra, and it is especially strong in the NLS1s. The origin of the optical Fe II lines, their excitation mechanisms, and the spatial location of the Fe II emission region in AGNs are still open questions (see, e.g., Popović et al. 2009; Kovačević et al. 2010; Popović & Kovačević 2011). There are also many correlations between Fe II emission and other AGN properties that require a physical explanation. As discussed above, we found that Fe II lines show a slightly better correlation with the continuum at 5100 Å than do Balmer lines (Figure 11). On the other hand, it seems that the Hβ line flux is better correlated with the Fe II emission than with Hα. We should note here that this better correlation might be caused by the fact that the Fe II fluxes are much more susceptible

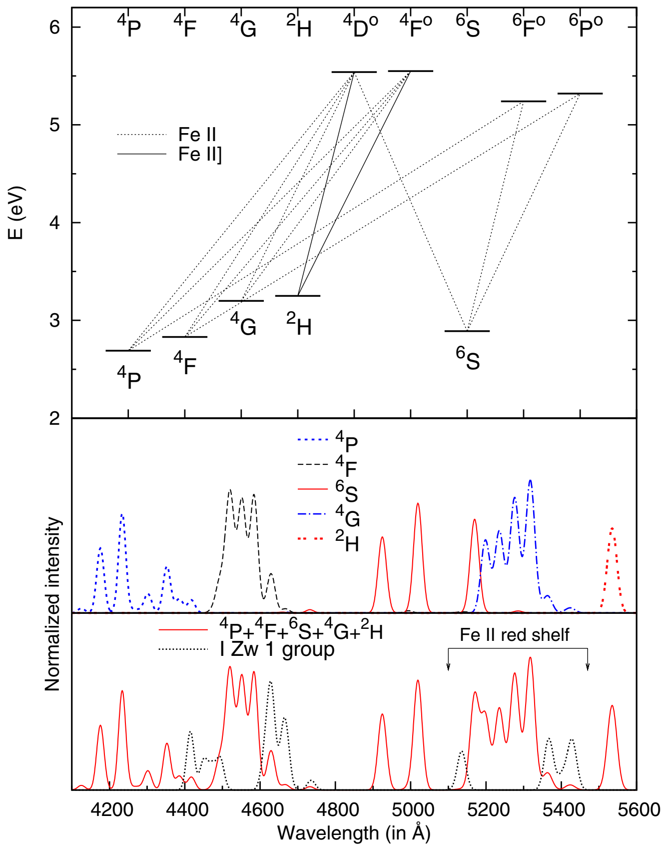

Figure 13. Simplified Grotrian diagram showing the strongest Fe II transitions in the λλ 4100–5600 region (top). Lines are separated into five groups according to the lower level of transition (middle): P (dotted line), F (dashed line), S (solid line), G (dash-dotted line), and H (double-dashed line). Bottom: the lines from the five line groups (solid line) and an additional line taken from I Zw 1 (see Kovačević et al. 2010), represented with dots. The measured red-shelf region is also noted (Table 4).

(A color version of this figure is available in the online journal.)

to contamination from the continuum emission than the Hα and Hβ lines are.

In order to explore the variability of Fe II lines in greater detail, we fitted the Fe II emission complex by the multi-Gaussian fitting method that Kovačević et al. (2010) and Popović & Kovačević (2011) described in detail. Our spectra cover a wider wavelength range (λλ4100–5600). Hence, simultaneous fits of the Fe II template and Hδ, Hγ, He II λ4686, and Hβ lines were carried out. In addition to the Fe II line template introduced in Kovačević et al. (2010), we included here 17 other Fe II lines, basically the transition arising from two groups with lower levels ^{4}P and ^{2}H[13] (see Figure 13 and Table 9).

An example of a best fit is presented in Figure 14, where all the strong emission lines and Fe II features are labeled. Since the Gaussian best fit includes a large number of free parameters (see Figure 14), we focused our attention on the fit required to reproduce the Fe II line emission as closely as possible. To this end, we first fit the strong hydrogen and helium lines and corrected their contribution to the Fe II lines. We then applied the best-fit procedure to the Fe II emission. With this scheme, we subtract the emission of all other lines and deal only with the Fe II spectrum (Figure 15). We fixed as many Gaussian parameters as possible, e.g., the ratio of [O III] lines or widths of the Balmer

Table 9
Line Transitions Added to the Fe II Template Given in Tables 1 and 2 of Kovačević et al. (2010)

Fe II Multiplet	Transition	Wavelength (Å)
Fe II 27-28	$b^4P_{5/2}$–$z^4F^o_{3/2}$	4087.284
	$b^4P_{5/2}$–$z^4F^o_{5/2}$	4122.668
	$b^4P_{5/2}$–$z^4D^o_{3/2}$	4128.748
	$b^4P_{5/2}$–$z^4D^o_{5/2}$	4173.461
	$b^4P_{5/2}$–$z^4F^o_{7/2}$	4178.862
	$b^4P_{5/2}$–$z^4D^o_{7/2}$	4233.172
	$b^4P_{3/2}$–$z^4F^o_{3/2}$	4258.154
	$b^4P_{3/2}$–$z^4D^o_{1/2}$	4273.326
	$b^4P_{3/2}$–$z^4F^o_{5/2}$	4296.572
	$b^4P_{3/2}$–$z^4D^o_{3/2}$	4303.176
	$b^4P_{3/2}$–$z^4D^o_{5/2}$	4351.769
	$b^4P_{1/2}$–$z^4F^o_{3/2}$	4369.411
	$b^4P_{1/2}$–$z^4D^o_{1/2}$	4385.387
	$b^4P_{1/2}$–$z^4D^o_{3/2}$	4416.830
	$b^4P_{5/2}$–$z^6F^o_{7/2}$	4670.182
Fe II] 55	$b^2H_{9/2}$–$z^4D^o_{7/2}$	5525.125
	$b^2H_{11/2}$–$z^4F^o_{9/2}$	5534.847

Notes. The atomic data are taken from the NIST atomic database.

line components NLR, intermediate-line region (ILR), and BLR (see also Zhang 2011). The line parameters inferred from our fits (width, shift, and intensity relative to total Hβ) are given in Table 10.

Kovačević et al. (2010) divided the Fe II emission into subgroups according to the lower level of the transition. We used the same criteria; thus, we considered here six line groups: ^{4}P, ^{4}F, ^{6}S, ^{4}G, ^{2}H, and I Zw 1. In Figure 16, we plot the fluxes of all these line groups, and the total Fe II emission in the 4100–5600 Å, against the continuum flux at 5100 Å. We omitted the ^{4}P group, since below 4200 Å the points are missing for more than 50% of the considered spectra, and the flux measurements for this group are therefore systematically lower. The total Fe II emission correlates well with the continuum ($r \sim 0.63$ and $P < 10^{-10}$). This correlation is slightly smaller than the one obtained for the measured Fe II in the wavelength region 5100–5470 Å (see Figure 11). The Fe ^{4}G line group consists of the transitions that contribute the most to the Fe II emission in the 5100–5470 Å range. For this line group, we obtained practically the same correlation with the continuum variation as was measured and presented in Figure 11 ($r \sim 0.74$ and $P < 10^{-16}$). A relatively good correlation ($r \sim 0.50$ and $P < 10^{-6}$) was obtained for the ^{4}G group (lines located in the blue part of the Fe II shelf) and for the high-excitation energy group I Zw 1 ($r \sim 0.56$ and $P < 10^{-8}$), while the other two groups have no correlation at all: Fe ^{2}H ($r \sim -0.01$ and $P = 0.82$) and Fe ^{6}S ($r \sim 0.14$ and $P = 0.18$). In the case of Fe ^{2}H, this could be due to the very weak emission coming from these transitions, while in Fe ^{6}S, it seems to be a real effect.

We compared the width of the Fe II lines to the widths of different Hβ components (Table 10). The average value of the Fe II lines is the same (within the error bars) as the average width value of the ILR component of the Hβ line (Figure 17). This clearly supports the idea that the origin of the Fe II emission is more likely within the ILR than the BLR, as stated before

[13] The atomic data were taken from the NIST atomic database: http://www.nist.gov

Table 10

The Line Parameters (w: widths; s: shifts; i: intensity[a]) from the Gaussian Best-Fitting of Hβ and Fe II Lines for 91 Good-Resolution Spectra

JD+ 2400000+ 1	w NLR (km s^{-1}) 2	s NLR (km s^{-1}) 3	i NLR (%) 4	w ILR (km s^{-1}) 5	s ILR (km s^{-1}) 6	i ILR (%) 7	w BLR (km s^{-1}) 8	s BLR (km s^{-1}) 9	i BLR (%) 10	w Fe II (km s^{-1}) 11	s Fe II (km s^{-1}) 12	i Fe II (%) 13
51424.4	525	36	0.21	1843	0	0.35	5493	0	0.44	1699	77	1.98
51425.4	504	20	0.20	1712	0	0.53	6238	−90	0.27	1627	6	1.90
51426.4	429	21	0.18	1534	0	0.48	5491	390	0.33	1347	125	1.62
51427.3	429	21	0.15	1538	0	0.48	5488	150	0.37	1694	19	2.30
51455.2	349	24	0.19	1578	0	0.60	5491	150	0.21	1602	3	2.14
51456.2	346	24	0.17	1443	30	0.54	6021	148	0.29	1398	56	1.55
51461.3	429	21	0.21	1560	0	0.57	3994	240	0.22	1450	−24	2.04
51465.2	409	15	0.17	1446	0	0.45	4995	−240	0.38	1497	−25	1.98
51485.3	409	15	0.16	1498	150	0.43	4992	0	0.41	1498	93	2.36
51486.2	409	15	0.15	1248	30	0.42	5241	90	0.43	1547	0	2.26
51487.2	409	15	0.16	1248	30	0.43	4992	0	0.41	1448	0	1.72
51488.2	409	15	0.16	1447	30	0.43	5491	0	0.41	1448	174	2.19
51489.2	409	15	0.15	1348	30	0.45	5491	0	0.40	1498	0	2.06
51513.2	409	15	0.15	1348	30	0.43	5491	0	0.42	1497	−22	2.26
51515.2	409	15	0.14	1348	30	0.41	5990	−450	0.44	1448	0	1.75
51693.5	410	101	0.16	1349	30	0.46	5489	300	0.39	1446	79	2.00
51702.4	449	30	0.15	1348	30	0.39	4992	0	0.46	1398	267	1.60
51734.4	450	30	0.17	1349	30	0.44	4998	−1	0.39	1499	173	2.27
51735.4	444	30	0.14	1348	30	0.36	5491	0	0.51	1547	0	2.43
51736.4	444	30	0.13	1298	30	0.33	5492	0	0.54	1547	180	2.03
51833.7	593	5	0.16	1548	−6	0.46	4968	0	0.37	1552	−66	1.97
52237.1	699	0	0.20	1467	60	0.45	5001	0	0.35	1714	21	2.14
52236.6	499	0	0.19	1548	0	0.42	4991	−30	0.39	1598	26	1.76
52501.8	540	15	0.19	1548	0	0.48	4992	−30	0.33	1497	−133	1.67
52589.7	474	0	0.19	1548	0	0.42	5492	−30	0.39	1497	17	1.75
52592.7	599	−42	0.14	1503	−101	0.45	5621	−98	0.40	1736	0	1.85
52618.6	444	18	0.20	1529	−41	0.48	4893	−33	0.33	1494	48	1.68
52620.6	700	1	0.17	1548	0	0.38	5490	−30	0.45	1647	1	2.16
52929.7	534	9	0.19	1454	31	0.40	4714	28	0.40	1539	12	1.77
52932.7	703	1	0.21	1549	0	0.46	4492	0	0.33	1597	41	1.92
52962.6	524	0	0.20	1448	30	0.41	4493	30	0.39	1547	−59	1.71
52990.6	500	15	0.21	1448	30	0.47	3993	30	0.32	1446	56	1.78
52993.6	849	30	0.21	1547	30	0.40	4993	60	0.39	1597	46	1.81
53234.9	749	27	0.21	1448	0	0.41	4743	0	0.37	1498	−49	1.84
53235.8	499	15	0.18	1447	30	0.43	4742	0	0.39	1448	−2	1.88
53237.9	749	27	0.20	1447	0	0.42	4795	15	0.38	1497	−29	1.95
53253.9	764	27	0.21	1443	−6	0.41	4840	20	0.38	1490	−34	1.84
53254.8	414	18	0.15	1260	30	0.44	4993	0	0.41	1647	14	1.77
53321.6	749	27	0.20	1448	0	0.43	4791	15	0.37	1498	−7	1.76
53326.6	599	15	0.20	1448	30	0.42	4742	0	0.38	1448	135	1.65
53327.6	749	27	0.18	1448	0	0.42	4793	15	0.40	1498	23	1.77
53352.6	649	27	0.18	1548	−60	0.41	4793	15	0.42	1597	−57	1.87
53353.6	499	15	0.20	1448	0	0.42	4741	0	0.38	1448	62	1.94
53495.0	397	15	0.18	1398	15	0.46	4986	16	0.36	1498	52	2.12
53608.9	699	0	0.21	1497	0	0.42	4742	15	0.36	1597	−44	2.11
53609.9	699	0	0.21	1498	0	0.42	4742	15	0.37	1597	3	1.90
53610.8	400	17	0.16	1347	0	0.46	4991	15	0.38	1548	−22	1.70
53611.8	404	24	0.16	1353	−1	0.45	4886	16	0.38	1518	−59	1.64
53612.8	433	19	0.17	1325	−6	0.43	5048	−34	0.40	1505	−92	1.62
53613.8	399	0	0.16	1332	−27	0.44	5091	15	0.40	1548	−90	1.64
53620.9	465	−14	0.17	1337	−60	0.43	5091	15	0.40	1497	−134	1.83
53622.9	464	−15	0.18	1278	0	0.42	4992	15	0.40	1498	2	1.86
53641.8	419	15	0.19	1278	0	0.42	4992	15	0.39	1498	−71	1.52
53643.8	414	22	0.16	1225	30	0.46	4992	0	0.39	1648	−19	1.76
53667.6	699	0	0.21	1497	0	0.42	4742	15	0.36	1597	−87	1.92
53669.7	419	0	0.17	1278	0	0.40	4991	15	0.42	1497	−5	1.81
53702.6	699	3	0.19	1298	0	0.40	4991	0	0.41	1498	−67	1.85
53703.6	449	12	0.19	1298	0	0.44	4992	0	0.37	1498	61	1.81
53710.6	364	12	0.15	1248	0	0.42	4991	15	0.43	1498	−20	1.80
53711.6	364	12	0.15	1248	0	0.42	4992	15	0.43	1497	0	1.80
53733.6	449	12	0.16	1248	0	0.47	4393	60	0.37	1498	−119	1.69
53974.9	649	0	0.19	1498	0	0.46	4742	15	0.35	1598	−67	1.84
53977.8	399	12	0.15	1248	0	0.40	5491	−300	0.44	1498	−9	1.62

Table 10
(Continued)

JD+ 2400000+ 1	w NLR (km s^{-1}) 2	s NLR (km s^{-1}) 3	i NLR (%) 4	w ILR (km s^{-1}) 5	s ILR (km s^{-1}) 6	i ILR (%) 7	w BLR (km s^{-1}) 8	s BLR (km s^{-1}) 9	i BLR (%) 10	w Fe II (km s^{-1}) 11	s Fe II (km s^{-1}) 12	i Fe II (%) 13
53978.8	649	0	0.19	1498	0	0.46	4743	15	0.35	1597	−37	1.87
53993.8	650	0	0.19	1497	0	0.46	4746	15	0.36	1598	−67	1.87
53995.7	650	15	0.19	1497	0	0.46	4741	15	0.35	1598	−92	1.90
53996.8	415	18	0.16	1263	30	0.43	4985	0	0.41	1601	−7	1.73
53997.8	639	15	0.19	1472	0	0.45	4742	15	0.36	1597	−75	1.84
54006.7	364	12	0.17	1248	0	0.48	4492	300	0.35	1397	19	1.90
54007.7	364	12	0.18	1247	0	0.48	4493	300	0.34	1397	6	1.83
54031.7	369	60	0.19	1148	90	0.43	4492	300	0.38	1398	248	2.01
54035.7	639	15	0.19	1473	0	0.45	4742	15	0.36	1597	−90	1.85
54036.7	405	20	0.18	1298	0	0.42	4992	0	0.40	1398	−8	1.58
54038.7	725	1	0.20	1470	0	0.44	4740	15	0.36	1600	−85	1.85
54039.7	401	3	0.16	1296	0	0.42	5001	−1	0.42	1399	−84	1.79
54069.6	599	0	0.19	1448	30	0.45	4743	15	0.37	1597	−57	2.07
54242.9	400	3	0.18	1297	0	0.42	5088	0	0.41	1450	8	1.92
54244.0	399	3	0.20	1298	0	0.45	4842	0	0.35	1447	−16	1.91
54322.9	604	0	0.20	1446	30	0.46	4740	15	0.35	1598	−26	1.86
54323.8	414	18	0.17	1306	30	0.43	4992	0	0.39	1547	−1	1.49
54346.8	399	3	0.20	1298	0	0.44	4493	0	0.36	1448	−6	1.63
54347.8	399	3	0.19	1298	0	0.41	4493	0	0.40	1447	−2	2.07
54350.9	606	0	0.21	1460	29	0.46	4488	14	0.33	1596	−65	1.77
54388.7	599	15	0.19	1448	30	0.47	4493	15	0.34	1598	−100	1.85
54390.6	400	3	0.20	1298	0	0.43	4243	150	0.37	1448	15	1.91
54391.7	399	3	0.18	1298	0	0.43	4493	150	0.40	1448	25	1.88
54405.7	399	3	0.18	1298	0	0.43	4493	150	0.39	1447	−15	1.86
54406.6	399	3	0.18	1298	0	0.43	4493	150	0.39	1448	−22	1.85
54407.6	599	15	0.21	1448	30	0.45	4493	15	0.34	1597	−49	2.01
54410.7	607	14	0.20	1451	30	0.45	4495	16	0.35	1595	−71	1.95
54412.6	399	3	0.17	1297	0	0.40	4993	0	0.42	1448	3	1.80
mean	507 ± 128	13 ± 16	0.18 ± 0.02	1404 ± 120	9 ± 28	0.44 ± 0.04	4938 ± 405	25 ± 109	0.38 ± 0.05	1523 ± 81	−2 ± 74	1.87 ± 0.19

Note. [a] The intensity is given as a ratio to the total Hβ (%), i.e., for Fe II it is the parameter R_{Fe}.

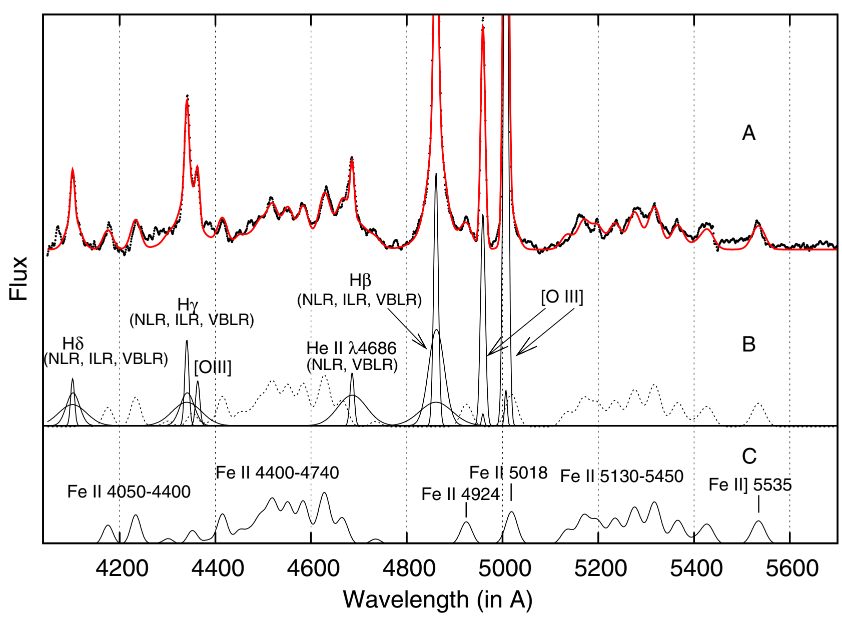

Figure 14. Example of the best fit (2001 November 23) of the λλ4000–5600 region: (A) the observed spectra (dots) and the best fit (solid line). (B) Hβ, Hγ, and Hδ fit with the sum of three Gaussians representing emission from the NLR, ILR, and BLR. The [O III] λλ4959, 5007 lines are fit with two Gaussians for each line of the doublet, and He II λ4686 is fit with one broad and one narrow Gaussian. The Fe II template is denoted with a dotted line and is also represented separately in region (C).
(A color version of this figure is available in the online journal.)

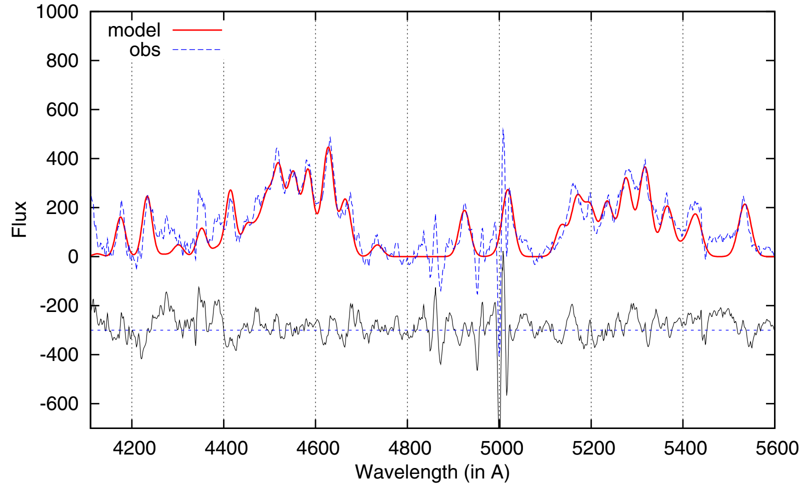

Figure 15. Example of the Fe II line emission (2001 November 23) in λλ4100–5600 cleared from the contamination of other strong lines in the field. The observed (dashed line) and fitted spectra (solid line) are shown. The bottom line represents the residuals.

(A color version of this figure is available in the online journal.)

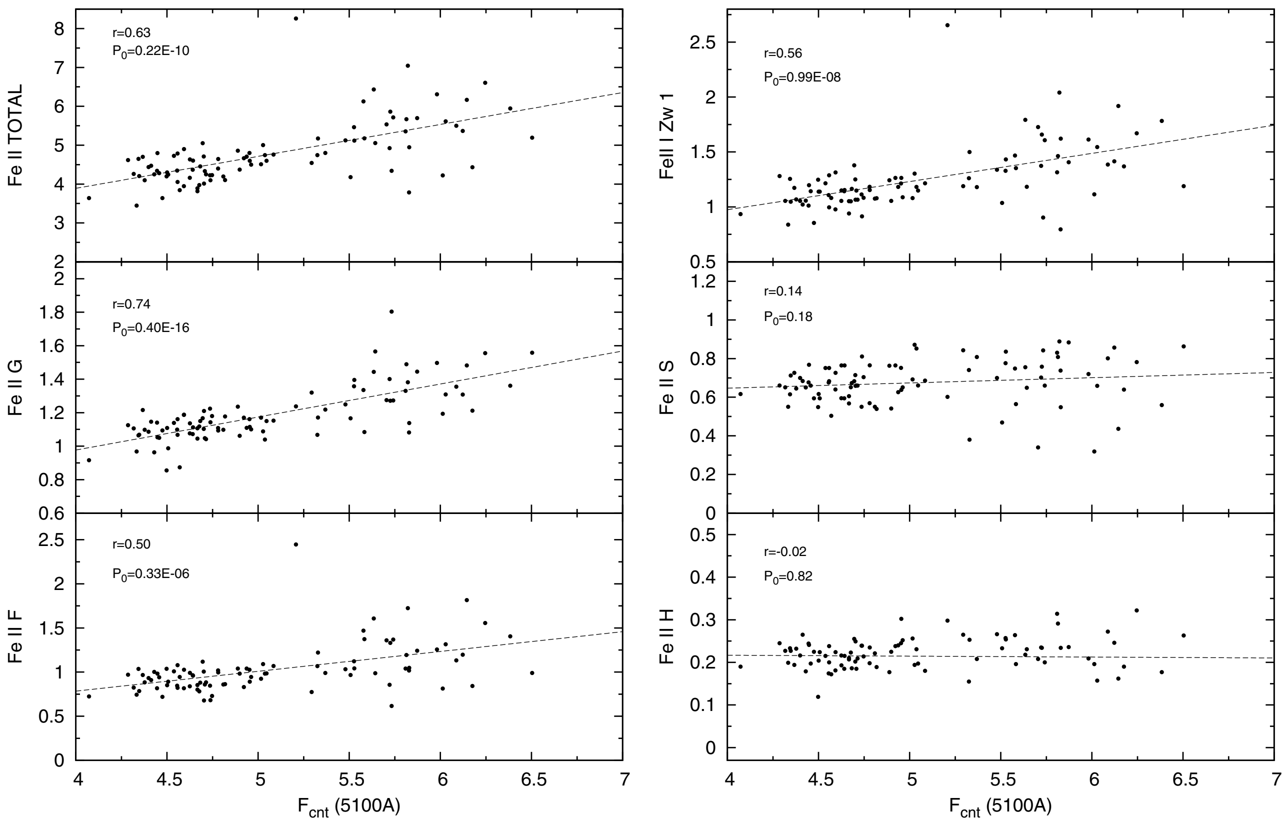

Figure 16. Fe II line fluxes (different groups and total fluxes) vs. continuum flux at 5100 Å. The correlation coefficient and the corresponding *P*-value are given in the upper left corner.

(see, e.g., Marziani & Sulentic 1993; Popović et al. 2004, 2009; Kovačević et al. 2010).

The quantity $R_{\rm Fe}$, defined as the flux ratio of optical Fe II emission to the Hβ line, is an important one in describing the EV1 parameter space (see Boroson & Green 1992). Here, the Hβ flux includes the contributions of all three components (narrow, intermediate, and broad), but still represents the behavior of the broad Hβ since the flux of the narrow component is expected to be constant. The variations of $R_{\rm Fe}$ as a function of the blue continuum flux are plotted in Figure 18. This plot shows a weak (statistically insignificant) but positive correlation between $R_{\rm Fe}$ and continuum flux (the correlation coefficient $r \sim 0.36$ and $P < 10^{-3}$).

6. DISCUSSION

6.1. The Structure of the Line-emitting Region in Ark 564

The permitted line profiles of Ark 564 are Lorentzian-like and can be found in a group of AGNs with an FWHM of broad lines smaller than 4000 km s^{-1} (Sulentic et al. 2009, 2011; Marziani et al. 2010). The problem is that such line profiles are not expected in the classical BLR. The Lorentzian-like line

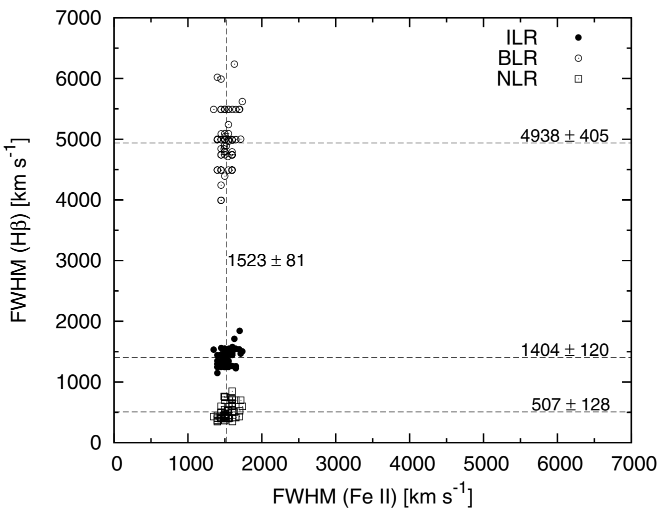

Figure 17. Gaussian widths of the Fe II lines compared with the widths of the Hβ ILR component. The vertical line shows the average value of Fe II widths, while the horizontal lines show the average values of the Hβ BLR, ILR, and NLR components.

profile can be caused by the composition of the three Gaussian profiles (as it was shown in Kovačević et al. 2010), where the contribution of the narrow component is significant. Contini et al. (2003), e.g., roughly estimated the contribution of the BLR to the total Hβ line and to the permitted lines in the UV and found that H$\beta_{\rm broad}$/H$\beta_{\rm narrow}$ should range between 1 and 2, which is not far from our estimation that the narrow component contributes to the total line flux with ∼20%. Also, Rodríguez-Ardila et al. (2000) showed that the flux carried out by the narrow component of Hβ in a sample of seven NLS1s is, on average, 50% of the total line flux. Therefore, such a high contribution of the narrow component to the total line flux can introduce a small rate of variation in broad lines, and the emission of the very broad component is very weak, i.e., a relatively small fraction of the total flux in the lines comes from the BLR.

The observed weak variation in the permitted lines of Ark 564 during a 10 year period is in agreement with a short-term monitoring covering a 2 year period given by Shemmer et al. (2001). They found no significant optical line variations. It is interesting that there is a weak correlation between the permitted lines and continuum variation. This, as well as the lack of correlation between Hα and Hβ, may indicate different sources of ionization, such as shock wave ionization in addition to photoionization. Moreover, five flare-like events (two prominent and three possible ones) were registered during the monitoring period; these confirm the flare-like variability reported in Collier et al. (2001) and indicate burst events in the emission line regions. These may indicate some kind of explosion (in starburst regions), which can additionally affect the line and continuum emission. The small [O III]/H$\beta_{\rm narrow}$ ratio may also indicate the presence of starbursts in the center of Ark 564 (as was noted for Mrk 493; see Popović et al. 2009).

Taking into account that it is very hard to properly decompose the narrow component (see discussion in Popović & Kovačević 2011, for more details) from the broad one, it is hard to discuss the geometry of the BLR of Ark 564. However, a lack of significant correlation between the Hα and Hβ flux variation may indicate that there is a very stratified (in physical parameters; see Section 4.1) emitting region, where the Hβ emitting region tend to be more compact than the Hα one. This idea is supported by the detected differences in the FWHM and

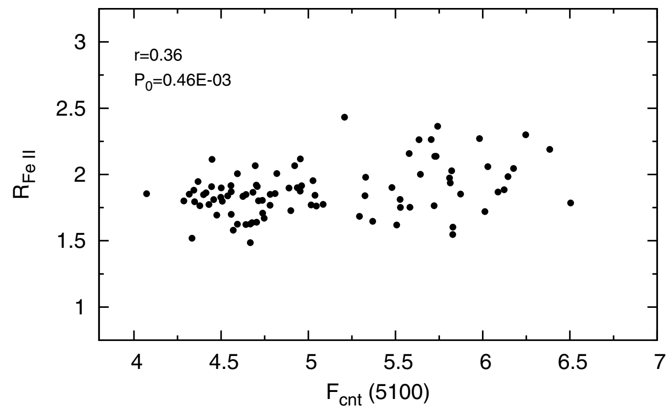

Figure 18. $R_{\rm Fe\,II}$ plotted against the blue continuum flux (EV1 parameter plane).

FW0I of Hα and Hβ and by the absent correlation between BD and continuum (Figure 8). On the other hand, the quasi-simultaneous variations of Hα and Hβ blue and red wings (Figure 6) and their good correlations (Figure 9) indicate a predominantly circular motion in the BLR.

We calculated the CCF and found a delay of only a couple of days. Taking the Hβ width and lag (assuming that the Hβ lag corresponds to the dimension of the BLR), one can estimate the mass of the black hole to be $\sim 1 \times 10^6$ solar masses, which is in agreement with previous estimates by Shemmer et al. (2001), Collier et al. (2001), and Pounds et al. (2001), and also well fits the hypothesis that NLS1s have lower black hole masses than typical Sy1s. However, one should take these estimates with caution, since there is no large correlation between the permitted lines and continuum variability. The CCF may indicate that the variability (perturbation) is coming from a relatively small region, but it is interesting that it causes amplification of the total line flux without significant change in line profiles (even during flare-like events). The permitted line profiles stay practically the same during the entire monitoring period (see Figure 7).

6.2. *Fe II Emission Variability in Ark 564*

The variability behavior of the Fe II complex in Seyfert galaxies has been poorly understood (see Collin & Joly 2000). Kollatschny et al. (2001), e.g., reported that in Mrk 110 the permitted optical Fe II complex remained constant within a 10% error over 10 years, while the forbidden [Fe X] λ6375 line was variable. Similarly, in the Seyfert 1 galaxy NGC 5548, no significant variations of the optical Fe II blends (less than 20%) were detected (Dietrich et al. 1993). However, the opposite result was reported in a long-term optical variability watch program on the Seyfert 1 galaxy NGC 7603 over a period of nearly 20 years (Kollatschny et al. 2000). This object displayed remarkable variability in the Fe II feature, with amplitudes of the same order as those for the Hα and He I lines. Giannuzzo & Stripe (1996) found that, out of 12 NLS1s, at least four presented significant variability of the Fe II complex with percentage variations larger than 30%. In addition, considerable variations of the Fe II emission (larger than 50%) were reported in two Seyfert 1 galaxies: Akn 120 and Fairall 9 (Kollatschny et al. 1981; Kollatschny & Fricke 1985). On the other hand, Kuehn et al. (2008) performed a reverberation analysis of the strong, variable optical Fe II emission bands in the spectrum of Ark 120; they were unable to measure a clear reverberation lag for these Fe II lines on any timescale. They concluded that the optical Fe II emission does not come from a photoionization-powered region similar in size to the Hβ-emitting region. Our results confirm this since for different groups there are different correlations with the continuum, and in some groups (as, e.g., ^{6}S) there is no correlation at all (see the discussion below).

The most interesting point is that the Fe II variation (at least in the red part of Fe II shelves) in Ark 564 is closely following the variations in the continuum. A similar result was obtained in the case of NGC 4051, an NLS1 galaxy, where the variability of the optical Fe II emission also followed the continuum variability (Wang et al. 2005).

We investigated the time variability of several Fe II multiplets in Ark 564. An interesting result is that there are different levels of correlations between the emission of Fe II line groups and continuum flux. It seems that the level of Fe II flux variability depends on the type of transition. For example, we registered a good correlation for ^{4}G and ^{4}F groups, which mainly contribute to the blue and red Fe II features around Hβ, and practically no significant correlation between ^{2}H and ^{6}S groups[14] and the continuum (Figure 13). The emission from these two groups seem to be variable, but there is no response to continuum variability. This may also indicate that the Fe II emission region in Ark 564 is stratified. On the other hand, the width of Fe II lines follows the width of the ILR component, which is in good agreement with results reported in previous work (Marziani & Sulentic 1993; Popović et al. 2004, 2009; Kovačević et al. 2010)

We found a positive (yet statistically insignificant) trend of $R_{\rm Fe}$ with the blue continuum. Wang et al. (2005) found a similar positive trend for the galaxy NGC 4051, in opposition to the negative trend observed in NGC 7603 (reported by Wang et al. 2005, on the data of Kollatschny et al. 2000). Comparing the variability behaviors of different objects, they argued that the objects with positive correlations have narrow Hβ lines and are consequently classified as NLS1s. The remaining two sources with negative correlations have relatively broad Hβ profiles. They interpreted that the dichotomy in variability behavior of $R_{\rm Fe}$ is due to the different physical conditions governing the variability of the optical Fe II emission. Our result is consistent with their findings, supporting their idea that in case of NLS1, the bulk excitation of the optical Fe II lines is due to collisional excitation in a high-density optically thick cloud illuminated and heated mainly by X-ray photons (see Wang et al. 2005, and references therein).

7. CONCLUSION

In this paper, we analyzed the long spectral variability of the NLS1 galaxy Ark 564, observed in the 11 year period from 1999 to 2010. We performed a detailed analysis of optical spectra covering the continuum flux at 5100 Å and 6200 Å, and Hβ, Hα, and Fe II lines. Here we briefly outline our conclusion:

1. In Ark 564 during the monitoring period (1999–2010) the mean continuum and line fluxes decreased ~20%–30% (see Figure 5) from the beginning (1999) to the end of the monitoring (2010). The total flux of Fe II evidently increases with the continuum flux.
2. We registered five flare-like events (two prominent and three possible) lasting ~1–3 days. During this period, fluxes in the continuum and lines changed ~20% (continuum and Fe II emission) and ~10% for Balmer lines.
3. The flux–flux correlations between the continuum and lines are weak, whereas the correlation between the Fe II lines (in the red shelf of the Fe II) and continuum is slightly higher (and more significant) than that between the Balmer lines and continuum. There is almost a lack of correlation between the Hα and Hβ line fluxes. Such behavior indicates very complex physical processes in the line-forming region, i.e., some additional physical processes besides the photoionization may be present.
4. We roughly estimated a lag of 2–6 days, but with large error bars. Given that the photoionization is probably not the only source of line excitation, the obtained results should be taken with caution.
5. We investigated in detail the Fe II emission variability. We divided the Fe II emission into six groups according to atomic transitions. We found that the correlation between the continuum flux and emission of groups depends on the type of transition, i.e., in some cases there is a relatively good correlation level between the Fe II group emission (^{4}G, ^{4}F group), but for ^{2}H and ^{6}S there is no correlation at all.
6. The Gaussian multicomponent analysis indicates that the emission of the Fe II lines probably comes from the ILR, having velocities around 1500 km s^{-1}.

The spectral variability of Ark 564 seems to be complex and different from that observed in BLS1 (see, e.g., Shapovalova et al. 2009). The observed flare-like events, the small (or even lack of) correlation between Hα and Hβ fluxes, the different correlation degree for Fe II group emission, and the continuum light level may indicate complex physics in the emitting regions, as, e.g., there may be, besides the AGN, contributions from star explosions and internal shock waves.

We thank the anonymous referee for very useful comments and suggestions. This work was supported by RFBR research grants N00-02-16272, N03-02-17123, 06-02-16843, N09-02-01136, and N12-02-01237a (Russia); CONACYT research grants 39560-F, 54480, and 151494 and PAPIIT-UNAM research grant IN111610 (México); and the project "Astrophysical Spectroscopy of Extragalactic Objects" (176001) supported by the Ministry of Education and Science of the Republic of Serbia. L.Č.P., W.K., D.I., and J.K. are grateful to the Alexander von Humboldt Foundation for support in the frame of program "Research Group Linkage."

REFERENCES

Alexander, T. 1997, in Astronomical Time Series, 218, ed. D. Maoz, A. Sternberg, & E. M. Leibowitz (Dordrecht: Kluwer), 163
Bischoff, K., & Kollatschny, W. 1999, A&A, 345, 49
Boller, Th., Brandt, W. N., & Fink, H. 1996, A&A, 305, 53
Boroson, T. A., & Green, R. F. 1992, ApJS, 80, 109
Collier, S., Crenshaw, D. M., Peterson, B. M., et al. 2001, ApJ, 561, 146
Collin, S., & Joly, M. 2000, New Astron. Rev., 44, 531
Contini, M., Rodríguez-Ardila, A., & Viegas, S. M. 2003, A&A, 408, 101
Crenshaw, D. M., Kraemer, S. B., Boggess, A., et al. 1999, ApJ, 516, 750
Crenshaw, D. M., Kraemer, S. B., Turner, T. J., et al. 2002, ApJ, 566, 187
Cruise, A. M., & Dodds, P. M. 1985, MNRAS, 215, 417
de Vaucouleurs, G., de Vaucouleurs, A., Corwin, H. G., Jr., et al. (ed.) 1991, Third Reference Catalogue of Bright Galaxies (New York: Springer)
Dietrich, M., Kollatschny, W., Peterson, B. M., et al. 1993, ApJ, 408, 416
Giannuzzo, E. M., & Stirpe, G. M. 1996, A&A, 314, 419
Hufnagel, B. R., & Bregman, J. N. 1992, ApJ, 386, 473
Hughes, P. A., Aller, H. D., & Aller, M. F. 1992, ApJ, 396, 469
Ilić, D., Popović, L. Č., La Mura, G., Ciroi, S., & Rafanelli, P. 2012, A&A, 543, A142
Kollatschny, W., Bischoff, K., & Dietrich, M. 2000, A&A, 361, 901

[14] Note that the ^{6}S Fe II group may be affected by the [O III] 5007 line; therefore, the lack of a correlation for this component might simply be due to measurement bias.

Kollatschny, W., Bischoff, K., Robinson, E. L., Welsh, W. F., & Hill, G. J. 2001, A&A, 379, 125
Kollatschny, W., & Fricke, K. J. 1985, A&A, 146, L11
Kollatschny, W., Schleicher, H., Fricke, K. J., & Yorke, H. W. 1981, A&A, 104, 198
Kovačević, J., Popović, L. Č., & Dimitrijević, M. S. 2010, ApJS, 189, 15
Kuehn, C. A., Baldwin, J. A., Peterson, B. M., & Korista, K. T. 2008, ApJ, 673, 69
Kuraszkiewicz, J. K., Green, P. J., Forster, K., et al. 2002, ApJS, 143, 257
Leighly, K. M. 1999a, ApJS, 125, 297
Leighly, K. M. 1999b, ApJS, 125, 317
Leighly, K. M. 2000, New Astron. Rev., 44, 395
Marziani, P., & Sulentic, J. W. 1993, ApJ, 558, 553
Marziani, P., Sulentic, J. W., Negrete, C. A., et al. 2010, MNRAS, 409, 1033
Matsumoto, C., Leighly, K. M., & Marshall, H. L. 2004, ApJ, 603, 456
O'Brien, P. T., Dietrich, M., Leighly, K., et al. 1998, ApJ, 509, 163
Osterbrock, D. E., & Pogge, R. W. 1985, ApJ, 297, 166
Panessa, F., de Rosa, A., Bassani, L., et al. 2011, MNRAS, 417, 2426
Peterson, B. M. 1993, PASP, 105, 247
Peterson, B. M., Barth, A. J., Berlind, P., et al. 1999, ApJ, 510, 659
Peterson, B. M., Berlind, P., Bertram, R., et al. 1994, ApJ, 425, 622
Peterson, B. M., Berlind, P., Bertram, R., et al. 2002, ApJ, 581, 197
Peterson, B. M., & Collins, G. W., II 1983, ApJ, 270, 71
Peterson, B. M., Pogge, R. W., Wanders, I., Smith, S. M., & Romanishin, W. 1995, PASP, 107, 579
Popović, L. Č., & Kovačević, J. 2011, ApJ, 738, 68
Popović, L. Č., Mediavilla, E., Bon, E., & Ilić, D. 2004, A&A, 423, 909
Popović, L. Č., Smirnova, A., Kovačević, J., Moiseev, A., & Afanasiev, V. 2009, AJ, 137, 3548
Pounds, K., Edelson, R., Markowitz, A., & Vaughan, S. 2001, ApJ, 550, 15
Rodríguez-Ardila, A., Pastoriza, M. G., Binette, L., & Donzelli, C. J. 2000, ApJ, 538, 581
Shapovalova, A. I., Doroshenko, V. T., Bochkarev, N. G., et al. 2004, A&A, 422, 925
Shapovalova, A. I., Popović, L. Č., Bochkarev, N. G., et al. 2009, NewAR, 53, 191
Shapovalova, A. I., Popović, L. Č., Chavushyan, V. H., et al. 2010, A&A, 517, A42
Shapovalova, A. I., Popović, L. Č., Collin, S., et al. 2008, A&A, 486, 99
Shemmer, O., Romano, P., Bertram, R., et al. 2001, ApJ, 561, 162
Smith, R. A. N., Page, M. J., & Branduardi-Raymont, G. 2008, A&A, 490, 103
Sulentic, J., Marziani, P., & Zamfir, S. 2011, Balt. Astron., 20, 427
Sulentic, J. W., Bachev, R., Marziani, P., Negrete, C. A., & Dultzin, D. 2007, ApJ, 666, 757
Sulentic, J. W., Marziani, P., & Zamfir, S. 2009, New Astron. Rev., 53, 198
Turner, T. J., Romano, P., George, I. M., et al. 2001, ApJ, 561, 131
Van Groningen, E., & Wanders, I. 1992, PASP, 104, 700
Wang, J., Wei, J. Y., & He, X. T. 2005, A&A, 436, 417
Zhang, X.-G. 2005, ApJ, 741, 104